NONUNIFORM MEMBRANES IN CAPACITIVE MICROMACHINED ULTRASONIC TRANSDUCERS

A THESIS
SUBMITTED TO THE DEPARTMENT OF ELECTRICAL AND ELECTRONICS ENGINEERING
AND THE INSTITUTE OF ENGINEERING AND SCIENCE
OF BILKENT UNIVERSITY
IN PARTIAL FULFILLMENT OF THE REQUIREMENTS
FOR THE DEGREE OF
MASTER OF SCIENCE

By
Muhammed N. Şenlik
January 28, 2005

I certify that I have read this thesis and that in my opinion it is fully adequate, in scope and in quality, as a thesis for the degree of Master of Science.

Prof. Dr. Abdullah Atalar (Supervisor)

I certify that I have read this thesis and that in my opinion it is fully adequate, in scope and in quality, as a thesis for the degree of Master of Science.

Prof. Dr. Hayrettin Köymen

I certify that I have read this thesis and that in my opinion it is fully adequate, in scope and in quality, as a thesis for the degree of Master of Science.

Assoc. Prof. Dr. Ahmet Oral

Approved for the Institute of Engineering and Science:

Prof. Dr. Mehmet Baray

Director of the Institute Engineering and Science in loving memory of my mother

ABSTRACT

NONUNIFORM MEMBRANES IN CAPACITIVE MICROMACHINED ULTRASONIC TRANSDUCERS

Muhammed N. Şenlik
M.S. in Electrical and Electronics Engineering
Supervisor: Prof. Dr. Abdullah Atalar
January 28, 2005

Capacitive micromachined ultrasonic transducers (cMUT) are used to receive and transmit ultrasonic signals. The device is constructed from many small, in the order of microns, circular membranes, which are connected in parallel. When they are immersed in water, the bandwidth of the cMUT is limited by the membrane's second resonance frequency, which causes an increase in the mechanical impedance of the membrane. In this thesis, we propose a new membrane shape to shift the second resonance frequency to higher values, in addition to keeping the impedance of the membrane as small as possible. The structure consists of a very thin membrane with a rigid mass at the center. The stiffness of the central region moves the second resonance to a higher frequency. This membrane configuration is shown to work better compared to conventionally used uniform membranes during both reception and transmission. The improvement in the bandwidth is more than %30 with an increase in the gain.

Keywords: Capacitive micromachined ultrasonic transducer, cMUT, nonuniform membrane.

ÖZET

KAPASİTİF MİKRO-İŞLENMİŞ ULTRASONİK ÇEVİRİCİLERDE DÜZGÜN OLMAYAN ZARLAR

Muhammed N. Şenlik
Elektrik ve Elektronik Mühendisliği, Yüksek Lisans
Tez Yöneticisi: Prof. Dr. Abdullah Atalar
28 Ocak 2005

Kapasitif mikro-işlenmiş ultrasonik çeviriciler (kMUÇ), ultrasonik sinyallerin alımında ve yollanmasında kullanılırlar. Cihaz mikron mertebesindeki birçok ufak zarın paralel bağlanmasıyla oluşturulur. Suda çalıştırıldıklarında, kMUÇ'un bant genişliği, zarın mekanik empedansının artmasına sebep olan, zarın ikinci rezonans frekansı ile sınırlıdır. Bu tezde ikinci rezonans frekansını zarın empedansını mümkün olduğunca ufak tutarak daha yukarı çıkaran yeni bir zar şekli öneriyoruz. Yapı ortasında sert bir kütle olan çok ince bir zardan oluşmaktadır. Ortadaki kısmın sertliği ikinci rezonansı daha yüksek frekanslara çıkarmaktadır. Bu zar yapısının alma ve yollama açısından şu an kullanılmakta olan zarlardan daha iyi olduğu gösterilmiştir. Bant genişliğindeki iyileşme kazançta artışla birlikte %30'dan daha fazladır.

Anahtar sözcükler: Kapasitif mikro-işlenmiş ultrasonik çevirici, kMUÇ, düzgün olmayan zar.

ACKNOWLEDGEMENTS

I would like to express my sincere gratitude to Dr. Abdullah Atalar for his supervision, guidance and encouragement through the development of this thesis.

I would like to thank to the members of my thesis jury for reading the manuscript and commenting on the thesis.

Endless thanks to Selim for useful discussions, always coming with a new idea to each meeting and the brilliant solutions to the problems we met.

Many thanks to my officemate, Onur Bakır. And I would like to express my sincere gratitude to the following people: Bozbey, Vahit, analog mates Mehmet and Çağrı, Ferhat (a.k.a. kırmızı), Ali Rıza (a.k.a. karanfil), Durukal, Hakan, Namık, Kamer, Apo, Deligöz.

Without my parents and aunt, this work would never be possible.

Finally, one another person, my brother, Servet deserves special thanks. Although I am the elder one, he was both a father and a mother for me since he came to Bilkent. Thanks for always being there.

Contents

List of Figures

Chapter 1

INTRODUCTION

Ultrasound, a rich field of study, found many applications in diverse areas ranging from nondestructive evaluation (NDE) to process control, cleaning to imaging [2, 3]. In most of the applications, piezoelectric materials are the first choice for constructing transducers [4]. In imaging applications, they work well in terms of both bandwidth and gain when the surrounding medium is solid. However, when they are immersed in a light medium[1] such as air and water, they have typically a low bandwidth due to the mismatch in acoustic impedances[2] and lack of proper matching layers, but still present high gain.

Recent advances in micromachining technology enabled the invention of capacitive micromachined ultrasonic transducer (cMUT), first reported in [6]. The device is constructed from a circular silicon nitride membrane suspended over silicon substrate with a small spacing, in sub-micrometer range, to form a capacitor. The impedance of the membrane is chosen to be low compared to the impedance of the immersion medium to increase the possibility of obtaining high bandwidth. However, they have small turns ratio[3] resulting in a small gain.

[1]Light medium is used for a medium having low acoustic impedance, which is defined as $Z_a = V_a \rho$ where V_a is the speed of sound in the medium and ρ is the density of the medium.

[2]Air and water have acoustic impedances of 400 kg/m^{2}s and 1.5×10^6 kg/m^{2}s, whereas a typical transducer impedance is 10×10^6 kg/m^{2}s [5].

[3]Turns ratio is used to determine the amount of conversion between the average velocity, a mechanical quantity, and the current, an electrical quantity, in an electromechanical system.

In a recent work [7], performance measures in terms of a gain-bandwidth product for both transmit and receive modes are defined. It is shown that a cMUT immersed in water can be optimized for both high gain and bandwidth for a given frequency range.

In this work, we show that the bandwidth of cMUT is limited by the antiresonance frequency of the membrane, which causes an increase in the membrane impedance. We find that use of a nonuniform membrane, a membrane with a rigid mass at the center, results in higher turns ratio and shifts the antiresonance frequency of the membrane to higher values without increasing the membrane impedance. Results are obtained for both uniform and nonuniform membranes for reception and transmission. They indicate that the nonuniform membranes are advantageous compared to the uniform ones in many aspects.

Chapter 2 gives the fundamentals and basic operation principles of cMUT. Chapter 3 introduces the tools that are used in modeling and simulations. Chapter 4 presents the results for various membrane configurations at different operation modes. The last chapter concludes this work.

Chapter 2

FUNDAMENTALS OF cMUT

In this chapter; capacitive micromachined ultrasonic transducer (cMUT) and its basic operation principles for different regimes are introduced. Underlying theory for cMUT is formulated. The chapter ends with some remarks regarding nonuniform membranes.

2.1 cMUTs

An ultrasonic transducer is used to receive and transmit ultrasonic signals. Most ultrasonic transducers are made up of piezoelectric materials [4]. When an electric field is applied to such a material, it changes its shape in response to applied field, hence creates an ultrasonic wave. Similarly, when its shape is changed, the electric field inside the material also changes, which corresponds to the detection of an ultrasonic wave. However, in terms of bandwidth in a light immersion medium such as air or water, integration with surrounding electronics and construction of transducer arrays, they have several drawbacks. Capacitive micromachined ultrasonic transducer (cMUT), first reported in [6], has advantages over their piezoelectric counterpart in terms of above considerations [8, 9, 10]. However, piezoelectric transducers have still higher gain compared to cMUTs due to their higher electromechanical coupling coefficient, k_T^2 [4, 11].

Fig. 2.1 shows 3D view of a single cMUT cell fabricated with the sacrificial layer method. The whole structure lies on silicon substrate, whose top is highly doped, which also acts as the ground electrode. Vibrating silicon nitride membrane is supported by silicon nitride stands. A metal (aluminum or gold) inside the membrane (whose position may vary) forms the top electrode. There is a thin silicon nitride insulator region above the substrate to prevent short circuits between the electrodes when membrane collapses. The gap that is formed inside the structure may or may not be sealed depending on the application. To increase the directivity and amount of received/transmitted power, many cMUTs are connected in parallel to form an array [12]. To fabricate cMUTs, there are two major methods, which are sacrificial layer [13, 14] and wafer bonding [15] methods. In wafer bonding method, silicon is used as the membrane material and silicon oxide is used as the insulator and stand.

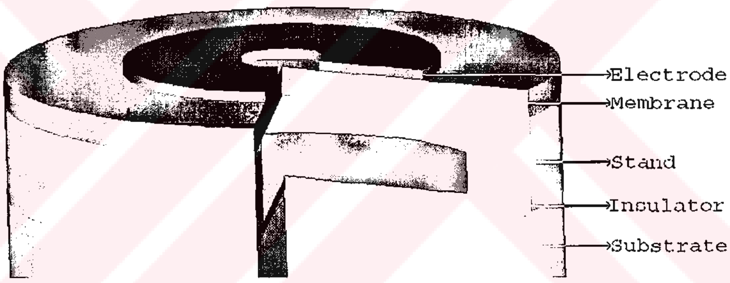

Figure 2.1: 3D view of a single cMUT cell fabricated with sacrificial layer method.

When a voltage is applied between the electrodes, regardless of the polarity, the membrane will deflect towards the substrate due to the attractive electrostatic forces. As the voltage is increased, the slope of the voltage-deflection curve also increases showing the increase of sensitivity with the applied voltage. At a critical point denoted as collapse voltage, V_{col}, the restoring forces of membrane can no longer resist the electrostatic forces and membrane collapses onto the insulator with a certain contact radius. Until the voltage is decreased to a critical value, V_{sb} the membrane contacts with the insulator and then it snaps back. Such a hysteresis behavior and membrane shapes for various voltages are

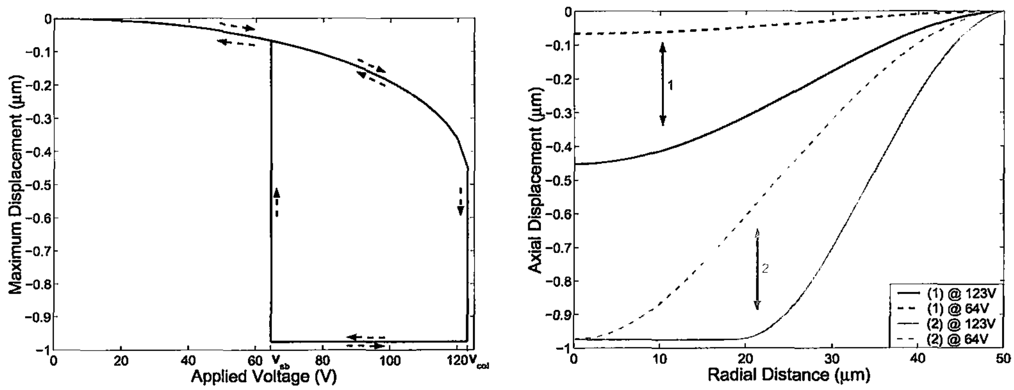

(a) (b)

Figure 2.2: (a) Deflection of the center of the membrane with respect to the applied voltage. Arrows indicate the direction of movement as the voltage is changed. (b) Membrane shapes for various voltages. Region denoted as '1' is before collapse and two membrane shapes at voltages just before collapse and after snap-back is drawn. Region '2' is after collapse and membrane shapes are drawn for just after collapse and before snap-back [1].

shown in Fig. 2.2(a)-(b). Results are obtained for a cMUT fabricated with sacrificial layer method. The membrane radius and thickness are 50 μm and 1 μm, respectively. The gap height and thickness of the insulator are 1 μm and 0.1 μm. Such a device has a V_{col} of 123 V and V_{sb} of 64 V.

2.2 Operating Principles and Regimes

Fig. 2.3 shows the cross-section of a cMUT. In this view, it is easy to see that cMUT is actually a parallel-plate capacitor formed between the top and bottom electrodes. In such a capacitor, the force resulting from the applied voltage, V, is given by

$$F_E = -\frac{1}{2}\frac{S\epsilon_0(\epsilon_{rm}\epsilon_{ri})^2}{(\epsilon_{rm}t_i + \epsilon_{rm}\epsilon_{ri}(t_g - y(r)) + \epsilon_{ri}t_e)^2}V^2 \tag{2.1}$$

where S is the area, t_i and t_g are the heights of the insulator and the gap, t_e is the electrode location with respect to the bottom of the membrane, ϵ_0 is

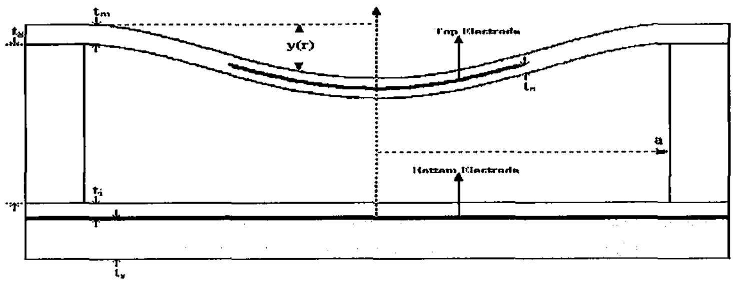

Figure 2.3: 2D view of a single cMUT cell fabricated with sacrificial layer method.

the permittivity of free space, and ϵ_{ri} and ϵ_{rm} are the relative permittivities of insulator and membrane material. Since the force (Eq. 2.1) is proportional to V^2; to avoid harmonic generation, a DC bias must be applied prior to operation. Hence the total applied voltage will be in the form of

$$V(t) = V_{DC} + V_{AC} sin(\omega t) \tag{2.2}$$

During the transmission, cMUT is driven with high amplitude AC voltage to couple more power to the medium. In receive mode, it is initially biased close to V_{col}. An incoming ultrasonic wave hits and vibrates the membrane. Such a vibration changes the total charge on the capacitor and creates a current across it.

2.2.1 Conventional Regime

In this regime, cMUT is operated such that it doesn't collapse [8]. Hence total operating voltage (Eq. 2.2) must be less than V_{col}. For higher sensitivity, cMUT is operated near V_{col} resulting in higher operating voltages. Although this situation is not a problem for receive mode; in transmit mode since cMUT must be driven with high AC to couple more power to surrounding medium; a high output pressure cannot be obtained without collapsing the membrane or increasing t_g. Despite these factors, conventional regime offers good linearity [16].

2.2.2 Collapsed Regime

This regime, recently proposed by Bayram *et all.* [1], leads to higher k_T^2 than the conventional regime. An initial voltage greater than V_{col} is applied resulting the membrane to collapse and cMUT is operated in this mode contacting with the insulator. During the operation, total voltage (Eq. 2.2) must be greater than V_{sb} to prevent cMUT to return to conventional mode. Depending on the applied voltage, the radius of the contact between the insulator and membrane changes and since this region is stationary, it is treated as a parasitic capacitance, which can be very high. Despite these, the collapsed regime provides a higher output pressure and linearity compared to the conventional regime [16].

2.3 Mathematical Formulation

cMUTs are typically fabricated in hexagonal shapes which allow close packing. However they can be successfully approximated with circular membranes clamped at their circumferences. The normal displacement of such a shape (Fig. 2.3) with radius a operating in vacuum under uniform pressure obeys the differential equation

$$\frac{(Y_0+T)t_m^3}{12(1-\sigma^2)}\nabla^4 y(r,t) - t_m T\nabla^2 y(r,t) - P + t_m\rho\frac{\partial^2 y(r,t)}{\partial t^2} = 0 \tag{2.3}$$

derived by Mason [17], where T is the residual stress, Y_0 is the Young's modulus, σ is the Poisson's ratio, ρ is the density of the membrane and P is the uniform pressure applied to the membrane. Under harmonic excitation using e^{jwt} notation, we obtain

$$\frac{(Y_0+T)t_m^3}{12(1-\sigma^2)}\nabla^4 y(r) - t_m T\nabla^2 y(r) - P - \omega^2 t_m\rho y(r) = 0 \tag{2.4}$$

To solve the equation (explicit spatial dependence of y has been left out), we need two boundary conditions which are

$$y(r)|_{r=a} = 0 \text{ and } \left.\frac{\mathrm{d}y(r)}{\mathrm{d}r}\right|_{r=a} = 0 \tag{2.5}$$

then the solution is given by

$$y(r) = \frac{P}{\omega^2 t_m \rho}\Big[\frac{-k_2 J_1(k_2 a) J_0(k_1 r) + k_1 J_1(k_1 a) J_0(k_2 r)}{-k_2 J_1(k_2 a) J_0(k_1 a) + k_1 J_1(k_1 a) J_0(k_2 a)} - 1\Big] \tag{2.6}$$

where J_0 and J_1 are the zeroth and first order Bessel functions of the 1st kind with

$$c = \frac{(Y_0 + T)t_m^2}{12(1-\sigma^2)\rho}\ ,\ d = \frac{T}{\rho} \tag{2.7}$$

and

$$k_1 = \sqrt{\frac{-d + \sqrt{d^2 + 4c\omega^2}}{2c}}\ ,\ k_2 = j\sqrt{\frac{d + \sqrt{d^2 + 4c\omega^2}}{2c}} \tag{2.8}$$

To complete the analysis, we have to find the mechanical impedance, Z_m. The mechanical impedance is defined as the ratio of applied uniform pressure to resulting average velocity which is

$$\begin{aligned} Z_m &= \frac{P}{\overline{v}} \\ &= j\omega l_t \rho\Big[\frac{a k_1 k_2(-k_2 J_1(k_2 a) J_0(k_1 a) + k_1 J_1(k_1 a) J_0(k_2 a))}{a k_1 k_2(-k_2 J_1(k_2 a) J_0(k_1 a) + k_1 J_1(k_1 a) J_0(k_2 a)) - 2(k_1^2 - k_2^2) J_1(k_1 a) J_1(k_2 a)}\Big] \end{aligned} \tag{2.9}$$

The first resonance (natural resonance) frequency, f_r, of membrane is given by

$$f_r = \frac{(2.4)^2}{2\pi}\sqrt{\frac{Y_0 + T}{12\rho(1-\sigma^2)}}\frac{t_m}{a^2} \tag{2.10}$$

The static deflection of membrane can be found by setting the time derivative term of Mason's differential equation Eq. 2.3 to 0 and solving the resulting equation. Then, the static displacement is calculated as

$$y(r) = \frac{P}{T}\Big[\frac{a[J_0(k_3 r) - J_0(k_3 a)]}{2k_3 J_1(k_3 a)} + \frac{a^2 - r^2}{4}\Big] \tag{2.11}$$

with

$$k_3 = \sqrt{\frac{T}{c t_m \rho}} \tag{2.12}$$

when the residual stress is neglected, $T \to 0$, the equation simplifies to

$$y(r) = \frac{12P(1-\sigma^2)}{Y_0 t_m^3}\Big[\frac{r^4 + a^4}{64} - \frac{a^2 r^2}{32}\Big] \tag{2.13}$$

The membrane collapses when the deflection of the center, $y(r=0)$, is

$$y(r)|_{r=0} = \frac{t_{eff}}{3} \tag{2.14}$$

where the effective gap height, t_{eff} is

$$t_{eff} = t_g + \frac{\epsilon_{rm} t_i + \epsilon_{ri} t_e}{\epsilon_{rm}\epsilon_{ri}} \tag{2.15}$$

and at that point collapse voltage, V_{col}, is

$$V_{col} = \sqrt{\frac{128 Y_0 t_m^3 t_{eff}^3}{36\epsilon_0(1-\sigma^2)a^4}} \tag{2.16}$$

Shunt input capacitance, C_0, is an important parameter that determines the performance of cMUT in terms of gain and bandwidth. It is formed between the top and bottom electrodes. It can be written in the integral form as

$$\begin{aligned} C_0 &\simeq \int_0^{2\pi}\int_0^{a+t_{eff}} \frac{\epsilon_0\epsilon_{rm}\epsilon_{ri}}{\epsilon_{rm} t_i + \epsilon_{rm}\epsilon_{ri}(t_g - y(r)) + \epsilon_{ri} t_e} r \mathrm{d}r \mathrm{d}\theta \\ &\simeq \frac{S'\epsilon_0\epsilon_{rm}\epsilon_{ri}}{\epsilon_{rm} t_i + \epsilon_{rm}\epsilon_{ri} t_{g0} + \epsilon_{ri} t_e} \end{aligned} \tag{2.17}$$

The extra capacitance due to the fringing fields is included by extending the radius from a to $a + t_{eff}$ [7] and S' is the corresponding membrane area. Approximation is performed under the assumption that all points of membrane deflected at the same amount which is $t_g - t_{g0}$. Since depending on the fabrication process; most of the cMUTs are fabricated with electrodes on top ($t_e = t_m$) or bottom ($t_e = 0$) of their membranes; C_0 of these limiting cases has great importance and is given by

$$C_0 \simeq \frac{S'\epsilon_0\epsilon_{rm}\epsilon_{ri}}{\epsilon_{rm} t_i + \epsilon_{rm}\epsilon_{ri} t_{g0} + \epsilon_{ri} t_m} \text{ and } C_0 \simeq \frac{S'\epsilon_{ri}}{t_i + \epsilon_{ri} t_{g0}} \tag{2.18}$$

for top and bottom electrodes.

Another important parameter for cMUT is the turns ratio, n, which denotes the conversion ratio between the electrical domain quantity, current and the mechanical domain one, velocity. For general case, it is given by

$$n = \frac{S'\epsilon_0(\epsilon_{rm}\epsilon_{ri})^2}{(\epsilon_{rm} t_i + \epsilon_{rm}\epsilon_{ri} t_{g0} + \epsilon_{ri} t_e)^2} V_{DC} \tag{2.19}$$

which can also be written as the product of C_0 and the electric field across the gap, E_{gap}, [18]

$$n = C_0 E_{gap} \tag{2.20}$$

with

$$E_{gap} = \frac{\epsilon_{rm}\epsilon_{ri}}{(\epsilon_{rm}t_i + \epsilon_{rm}\epsilon_{ri}t_{g0} + \epsilon_{ri}t_e)^2}V_{DC} \tag{2.21}$$

For top and bottom electrodes configurations, n simplifies to

$$n \simeq \frac{S'\epsilon_0(\epsilon_{rm}\epsilon_{ri})^2}{(\epsilon_{rm}t_i + \epsilon_{rm}\epsilon_{ri}t_{g0} + \epsilon_{ri}t_m)^2}V_{DC} \text{ and } n \simeq \frac{S'\epsilon_0\epsilon_{rm}^2}{(t_i + \epsilon_{ri}t_{g0})^2}V_{DC} \tag{2.22}$$

2.4 Nonuniform Membranes

Capacitive transducers with nonuniform membranes have been used for condenser microphones and pressure sensors [19, 20]. If we apply the same approach to a cMUT, we have a circular membrane clamped at its perimeter with a rigid mass at the center. Since all points on the mass move with the same velocity, resulting n will be considerably higher compared to a uniform membrane. Fig. 2.4(a)-

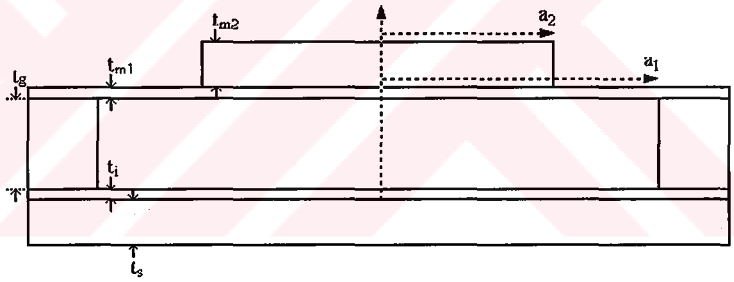

(a)

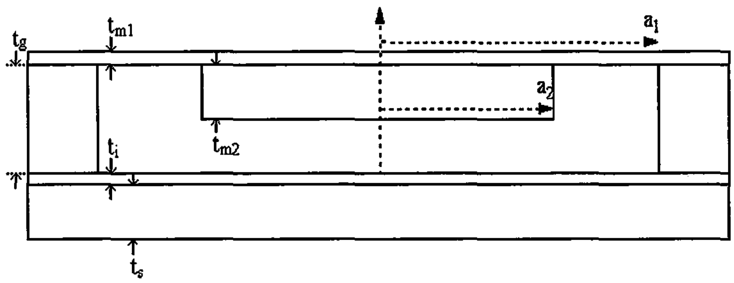

(b)

Figure 2.4: 2D view of a single cMUT cell with nonuniform membrane suited for fabrication with (a) the sacrificial layer method. (b) the wafer bonding method.

(b) shows cMUTs with nonuniform membranes suited for different fabrication methods. The radius and thickness of the mass at the middle of the membrane are a_2 and $(t_{m1} + t_{m2})$. The radius of the uniform part is a_1.

Nonuniform membranes have an antiresonance frequency, f_a, considerably higher than the uniform membrane by preventing the deflections due to the second resonance. However, Z_m can easily assume very high values with a certain choices of membrane dimensions. The structure can be approximated with a first order model, modeling only the first resonance, which is the series combination of a spring and a mass. The electrostatic force exerted by the capacitor is denoted as F_E[1] (Fig. 2.5). Here, the restoring force of the membrane is assumed to be a linear function of displacement and represented by a spring with constant k, corresponding the thin region around the mass. The mass represents the mass of the membrane.

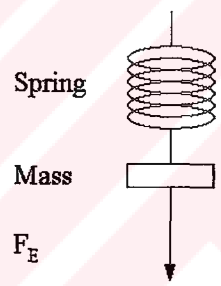

Figure 2.5: First order model, a series combination of a spring and a mass system.

In this work, all cMUTs are assumed to be fabricated with the sacrificial layer method. Hence the membrane, stand and the insulator are constructed from silicon nitride, whereas substrate is made of silicon. The electrode is assumed to be at the bottom of the membrane ($t_e = 0$).

[1] This simple approximation is also suited for most of the electromechanical systems in addition to cMUTs.

Chapter 3

MODELING

Equivalent circuits are powerful tools to predict the static and dynamic behavior of electromechanical systems [21]. A small signal equivalent circuit (Mason's equivalent circuit) is proven to work correctly for cMUTs when operated in vacuum or a light medium such as air [8, 18]. The impedance of the loading medium is treated as a lumped real impedance given by the product of the area of the transducer with the acoustic impedance of the medium. However, such a modeling of the surrounding medium, if its acoustic impedance is high (as in the case of water) is not enough and results in inaccurate modeling [22, 23].

First small signal equivalent circuit used in both transmit and receive is introduced and its elements are discussed briefly. Then, the finite element model used in simulations is described. The model is verified by comparing the results with the theoretically expected ones.

3.1 Small Signal Equivalent Circuit

In the receive mode, cMUT is biased close to its collapse voltage for higher sensitivity (Fig. 2.2(a)). When the wave hits cMUT, it causes the membrane to vibrate. Such a vibration causes the total charge across the capacitor to change and results in the creation of an AC current. In the transmit mode, to couple more power to surrounding medium, cMUT is driven with high amplitude AC voltage. (Usually in transmit mode, to overcome the effect of the attractive electrostatic forces during the release of membrane; cMUT is only driven with square voltage whose offset is used as bias voltage.) Such a case results in the generation of higher order harmonics and decrease the expected pressure value in the medium. Although it is reasonable to use a large-signal equivalent circuit [24], in this work small-signal equivalent circuit with few approximations is used to predict the transmit behavior.

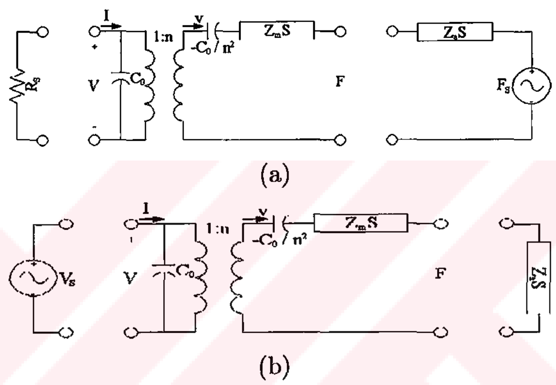

Figure 3.1: Mason model (a) for a cMUT operating as a receiver excited by the acoustical source (F_S, Z_aS) to drive the electrical load resistance of the receiver circuitry (R_S) (b) for a cMUT operating as a transmitter excited by a voltage source (V_S) to drive the acoustic impedance of the immersion medium (Z_aS). S is the area of the transducer

Fig. 3.1 shows the small signal equivalent circuits also known as the Mason's equivalent circuit for transmission and reception. Since the incoming wave is small in amplitude and cMUT can be linearized around bias point, this circuit is valid for small signal analysis of cMUT. Each element of equivalent circuit is described next and the formulas given in the previous chapter for bottom electrode case is repeated.

Shunt Input Capacitance, C_0, denotes the capacitance that forms between the electrodes of cMUT. As shown in Eq. 2.21, an increase in C_0 brings an increase in the turns ratio. However, C_0 also restricts the bandwidth of the device. Hence, the relation between C_0, n and bandwidth is quite complex. For bottom electrode, it is approximated as

$$C_0 \simeq \frac{S'\epsilon_{ri}}{t_i + \epsilon_{ri} t_{g0}} \tag{3.1}$$

Transformer and Turns Ratio, n, the heart of the device operation is performed by the transformer, since it converts the electrical domain quantity, current (I), to its analogue in the mechanical domain, which is average velocity ($\overline{v}$) (since there is a conversion between the mechanical and electrical domains, the device is an electromechanical transducer). The ratio between the conversion is given by the turns ratio, n,

$$n \simeq \frac{S'\epsilon_0 \epsilon_{rm}^2}{(t_i + \epsilon_{ri} t_{g0})^2} V_{DC} \tag{3.2}$$

Negative Capacitance, $-C_0/n^2$, as the applied DC bias is increased, the resonance frequency of the membrane decreases. This phenomena is called the spring softening effect and in the equivalent circuit, by using a negative capacitance series to mechanical impedance of the membrane, it is taken into account.

Lumped Mechanical Impedance, $Z_m S$, when a force is applied to the membrane, it shows response to applied force. Such a force shows itself in terms of mechanical impedance. Its definition is given by the ratio of the uniform applied pressure to the resulting average velocity ($Z_m = P/\overline{v}$). As in the case of piezoelectric transducers [4], the impedance can be written as infinite summation of series and parallel LC circuits. However, most of the time, it is reasonable to model the impedance around the natural resonance as series LC and antiresonance as parallel LC. Since lumped impedance is mentioned, Z_m is multiplied with transducer area, S, to find the lumped value.

Lumped Medium Impedance, $Z_a S$, the impedance of the surrounding medium is treated as the real lumped impedance and given by the product of the specific acoustic impedance, defined as the multiplication of density of the medium with the speed of sound in medium $Z_a = \rho V_{sonc}$, and transducer area. Such a treatment doesn't take into account the hydrodynamic loading of medium. Although using the radiation impedance can be a solution, as shown by [22], it is not enough.

The theoretical results are approximate and don't take the *DC* bias when calculating the mechanical impedance. It is necessary to obtain the equivalent circuit parameters by performing a finite element simulation.

3.2 Finite Element Model

Finite element simulations are required to obtain the parameters and solve the problems of equivalent circuit discussed previously. ANSYS^{TM}, which is a commercially available finite element package capable of solving electrostatic and structural problems, is used. First a circular membrane is modeled and solved. The results are compared with the theoretical ones to check the validity of simulations.

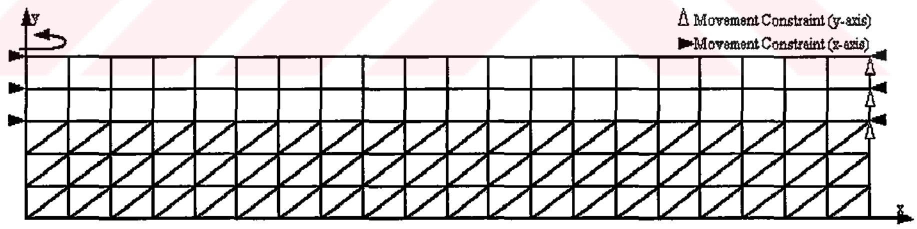

Figure 3.2: Circular membrane meshed with quadrilateral elements clamped at its perimeter.

Fig. 3.2 shows a circular membrane meshed with quadrilateral elements clamped at its perimeter. The region under the membrane is meshed with triangular elements for re-meshing ease. The axis-symmetric option, which denotes 360^0 rotation around the symmetry axis passing through the center, of the elements used in the simulations is enabled; hence only the cross-section of the membrane is modeled.

The test model used for FE verification has a radius, a, and thickness, t_m, of 50 μm and 1 μm. The membrane material is silicon nitride. Gap height, t_g, is 1 μm. First, a sinusoidally varying uniform pressure (100 Pa), $P\sin(\omega t)$ between 1.5 MHz and 2.5 MHz, is applied to the membrane. In all simulations residual tension, T is taken to be 0. Fig. 3.3(a) shows the resulting maximum displacement at 2.5 MHz obtained from theoretical calculations and FE simulations. There is an excellent agrement between theoretically expected results and finite element simulations. The second step is to determine the mechanical impedance of the membrane. By following the definition in Eq. 2.9, a small uniform pressure, P, is applied to the membrane and resulting average velocity, $\overline{v}$, is calculated. Then $P/\overline{v}$ gives the mechanical impedance (Fig. 3.3(b)). Again there is an excellent agrement between the theoretical results and FE simulations.

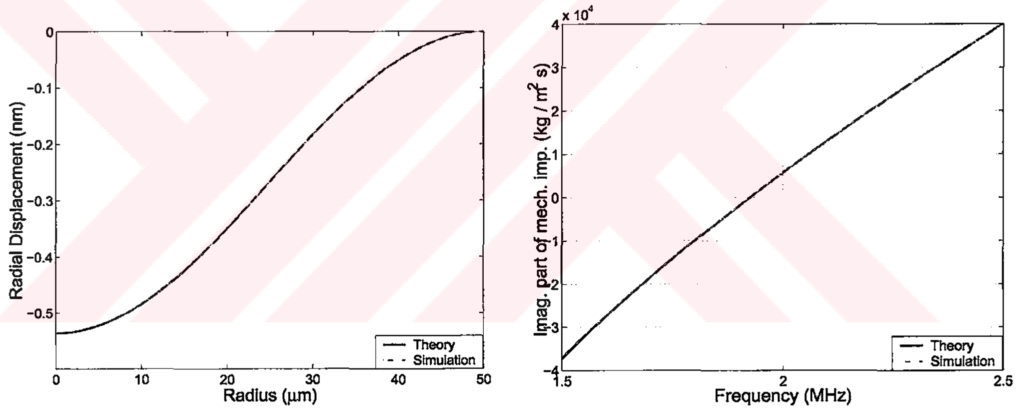

(a) (b)

Figure 3.3: (a) Maximum deflection of membrane under sinusoidally varying uniform pressure (for 100 Pa at 2.5 MHz). (b) Mechanical impedance of the membrane.

The solution of membrane shape for applied DC voltage must be handled carefully since it involves two domains, namely electrical and mechanical. The electrostatic and structural problems are solved separately. When a voltage is applied to the membrane, the resulting electrostatic field and the force due to the voltage distribution can be solved. Then those forces are applied to the membrane which results in deformation of the shape. However, such a deformation alters the electrostatic problem which must be resolved. This iterative approach continues until a convergence criteria (based on the maximum displacement) is reached. Since in the first iteration, voltage is applied to un-deformed membrane (so the electrostatic simulation results in uniform electric field), it can be used to check the DC deflection formula, Eq. 2.13. Fig. 3.4(a) shows a membrane shape for a converged solution obtained at 120 V. The first iteration result agrees well with the theoretical one. When the solution doesn't converge (Fig. 3.4(b)), it

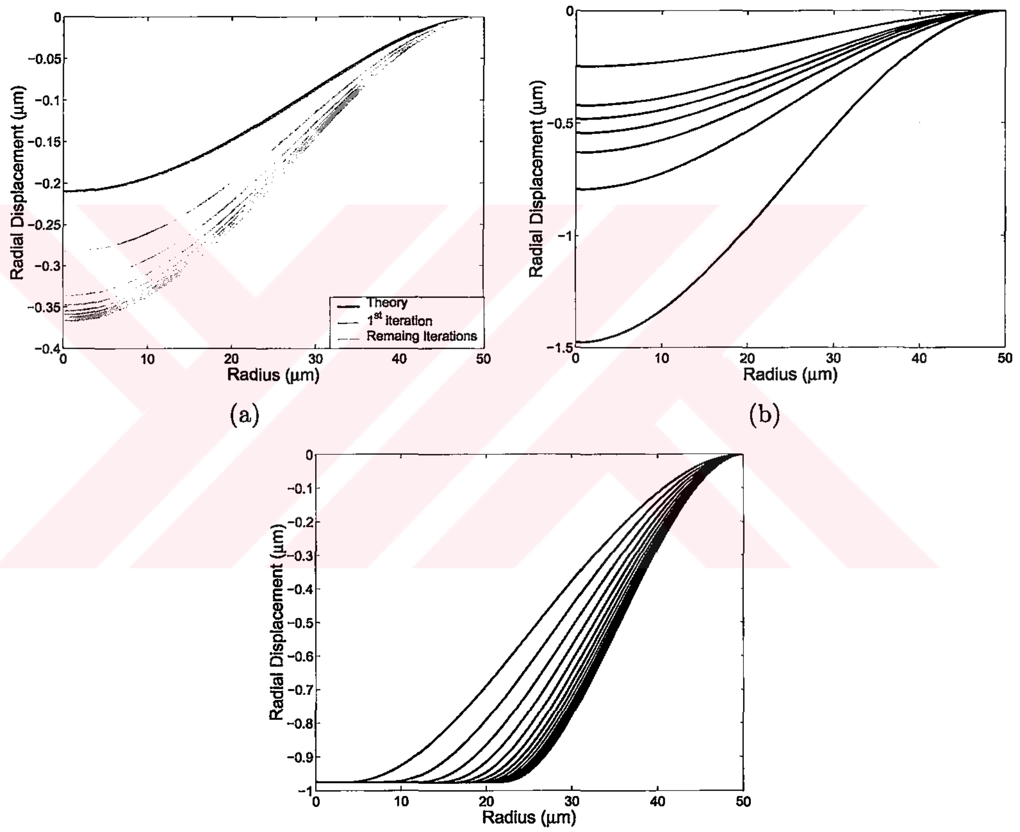

Figure 3.4: Iterative solution of membrane shape under various operating voltages (a) Converged solution at 120 V. (b) Un-converged (collapsed) solution at 130 V in conventional regimes. (c) Converged solution at 130 V in collapsed regime.

denotes the collapse of membrane at 130 V. Such an approach is valid only when the membrane is operating in the conventional regime. To find the membrane shape when it collapses, a preliminary simulation as described above to find V_{col} must be performed. Then, the center of the un-deformed membrane is displaced an amount of %95 of gap height (such an offset is required for meshing ease) and the resulting structural problem is solved which gives the new finite element model. The remaining steps are the same as the previously described approach. An energy based convergence criteria is used. Fig. 3.4(c) shows the resulting membrane shape for collapsed membrane at 130 V.

cMUT requires a more complete model than a simple circular membrane. Substrate, insulator and stand must also be modeled. Fig. 3.5 shows the cMUT model used in simulations. In simulations, the effect of the immersion medium is not included.

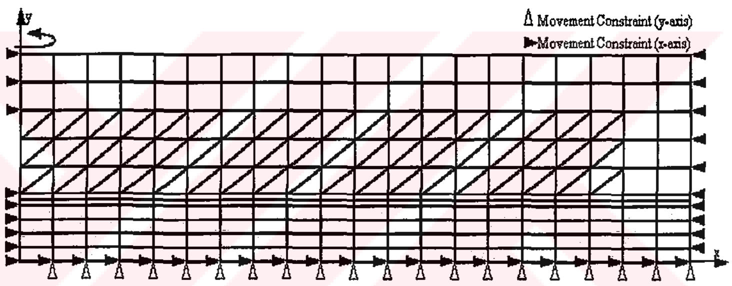

Figure 3.5: cMUT model used in simulations.

Chapter 4

RESULTS AND DISCUSSIONS

In this chapter, cMUTs having uniform and nonuniform membranes are compared using the performance measures defined in [7] for both receive and transmit modes when cMUT is immersed in water. Those performance measures are advantageous, since they enable monitoring both the gain and the bandwidth of the transducer. The tradeoff between these two is shown by changing various parameters of the device, namely the gap height (t_g), and axial membrane dimensions (a, a_1 and a_2), (t_m, t_{m1} and t_{m2}) and the termination at the electrical side (R_S). Each of these parameters are optimized for different membrane configurations and operation modes.

The chapter begins with the investigation of effect of the electrode size on the shunt input capacitance (C_0), turns ratio (n) and collapse voltage (V_{col}) of the device. A suitable pattern is proposed for both of the membrane types, without changing n and V_{col}, but with a reduced C_0. To make a fair comparison between the performance of the devices later in the chapter, the natural resonance frequencies, f_r, of the membranes are held constant, hence the chapter continues with the results showing the change of f_r and the antiresonance frequency, f_a, of the membranes with respect to different membrane dimensions. The remaining of the chapter is devoted to the definitions of figure of merits for both receive, M_R, and transmit, M_T, modes and the comparison of the membranes. Each of the results are obtained by conducting finite element (FE) simulations.

4.1 Electrode Patterning

The thickness of the electrode, its location inside the membrane and position with respect to the center influence the values of the equivalent circuit parameters [25, 26]. From Eq. 2.21, it is seen that n depends on the electric field across the gap and the field inside the membrane is ineffective. Hence to prevent the unnecessary use of the voltage inside the membrane, it is reasonable to place the electrode to the bottom of the membrane (Referring to Fig. 2.3, $t_e = 0$.). In all simulations, the electrode is assumed to be at the bottom of the membrane with an infinitely small thickness. The electrode covers the central region of the membrane with a certain radius. C_0 and n is obtained when the device is biased at %90 of its V_{col}.

C_0 is an important parameter that limits the gain and determines the lower end of the bandwidth of the transducer, although it increases n (Eq. 2.21). [26] showed that if the breakdown fields occurring in the device is ignored, the maximum bandwidth can be achieved with an infinitely small electrode located at the center of the membrane with an infinitely high voltage at the expense of reduced n, however still having maximum gain[1]. Although such a configuration is not possible; in [26], it is also shown that when the electrode radius is equal to the half of the membrane radius, it is possible to decrease C_0 without changing n and V_{col}. The fringing fields of the electrode causes V_{col} not to change and the outermost region of the membrane cannot contribute to n (while increasing C_0), since those regions are clamped at the perimeter. The results are repeated for a membrane with a and t_m equal to 25 μm and 0.74 μm respectively with $t_g = 0.25$ μm and can be seen in Fig. 4.1. As it can be seen in the figure, when the radius of the electrode is %70 of the a, V_{col} and n remains same, whereas C_0 decreases more than %40[2].

Similar to the uniform membrane case, an electrode pattern that is suited for the nonuniform membrane can also be found. If the electrode covers only

[1] In this work, the mechanical impedance of the membrane, Z_m, is assumed to be small compared to the acoustic impedance of the water and is not included in the calculations. A matching network is used at the electrical side to obtain the maximum gain, 0 dB.

[2] The difference between the presented results and [26] is due to applied bias voltage to obtain the equivalent circuit parameters.

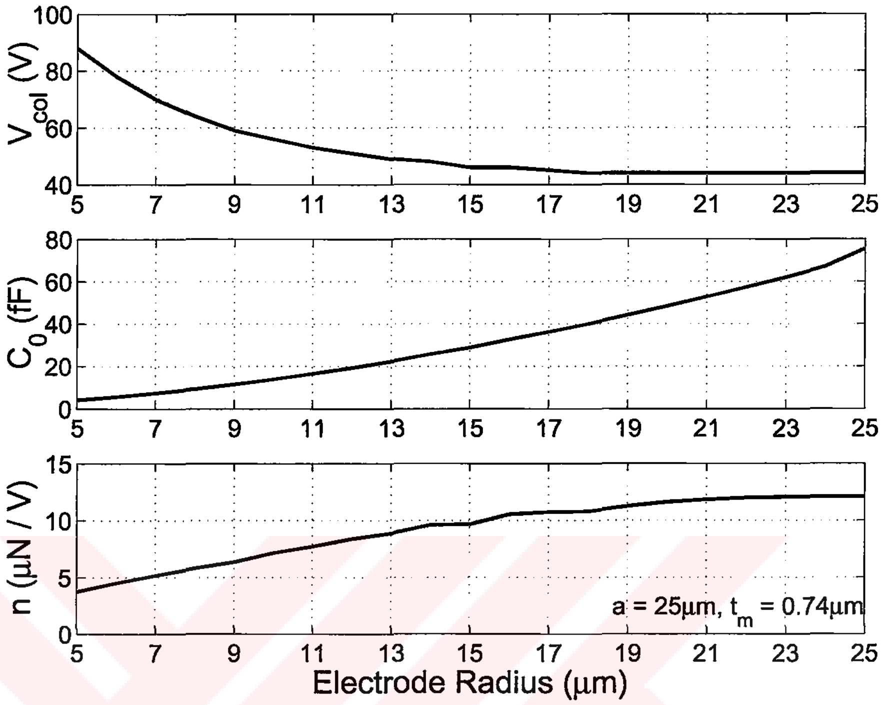

Figure 4.1: Change of V_{col}, C_0 and n with respect to the electrode size for the uniform membrane.

the nonuniform part of the membrane, it is still possible to decrease C_0 without affecting the remaining parameters. Results for a nonuniform membrane with a_1, a_2, t_{m1} and t_{m2} equal to 25 μm, 18.5 μm, 0.44 μm and 1.8 μm are shown in Fig. 4.2. The decrease in C_0 is approximately %40 without changing n and V_{col}.

4.2 Resonance Frequency Change

Natural resonance (first resonance, f_r) and antiresonance (second resonance, f_a) frequencies are important parameters that effect the performance of cMUT. In immersion transducers, the maximum pressure, P, occurs at f_r and the higher end of the bandwidth is determined by f_a. Both of these are strongly affected by the operating voltage (spring softening effect) and the hydrodynamic mass of the

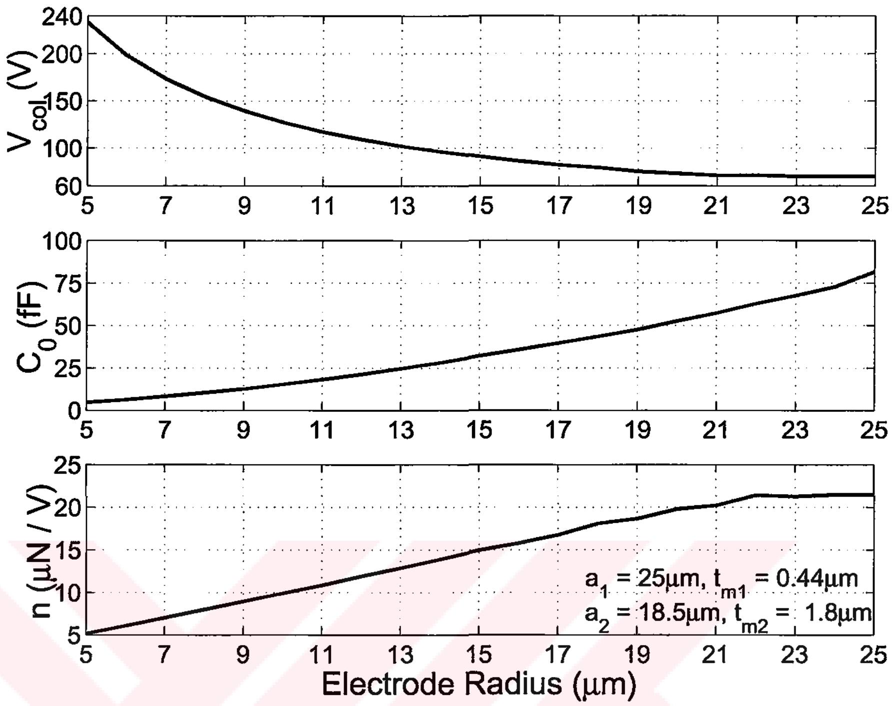

Figure 4.2: Change of V_{col}, C_0 and n with respect to the electrode size for the nonuniform membrane.

water, which brings additional imaginary load on the membrane. In this work, hydrodynamic mass is not modeled.

The modal shapes of the uniform membrane at f_r and f_a can be seen in Fig. 4.3[3]. Results are obtained for $a = 26$ μm and $t_m = 0.8$ μm. Corresponding resonance frequencies are 5.5 MHz and 18 MHz. A closer look to the figure

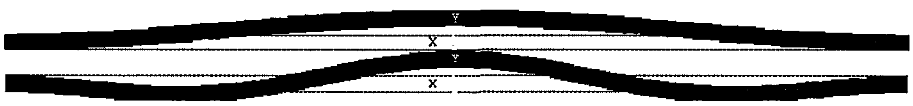

Figure 4.3: Modal shapes of the uniform membrane at f_r (upper one) and f_a (lower one).

[3]In this section, it is assumed that no bias is applied to the device, hence spring softening has no influence on the f_r and f_a of the membranes.

indicates that at f_r, all the points on the membrane deflect at the same direction, whereas at f_a, the central region of the membrane deflects at the opposite direction compared to remaining parts. As shown in Eq. 2.10, f_r of the uniform membrane is proportional to a/t_m^2, which can also be seen in Fig. 4.4. From the figure, it is seen that f_a also shows same type of behavior. The results are obtained when a is held constant at 26 μm and t_m is continuously increased.

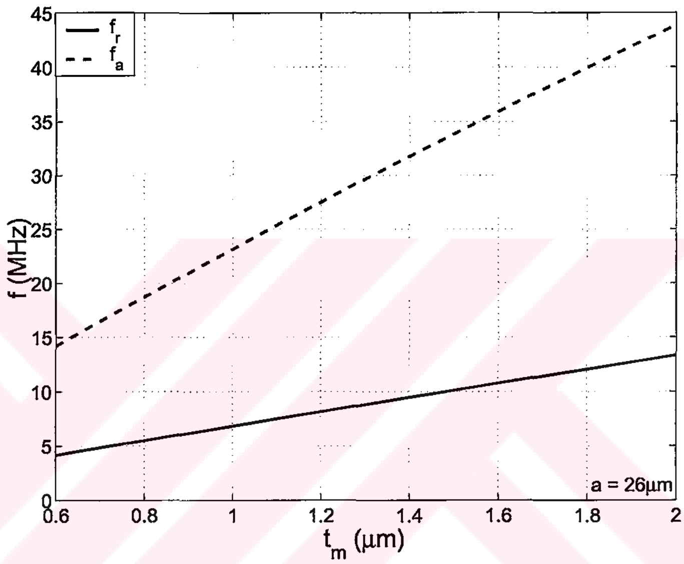

Figure 4.4: Change of f_r and f_a of the uniform membrane with respect to t_m for constant a.

It is critical to increase f_a without changing f_r, since it prevents the possibility of obtaining higher bandwidths. Again referring to Fig. 4.3, one solution will be to force the central region to bend in the same direction with the remaining portion at the actual f_a. This can be achieved, if we put a mass to the center of the membrane (equivalently increasing the thickness of the central region), forming a nonuniform membrane. By making such a modification, actually we are increasing the effective stiffness of the central region of a uniform membrane rather than increasing its density. Modal shapes of such a configuration can be seen in Fig. 4.5. Referring to Fig. 2.4(a), a nonuniform membrane with $a_1 = 25$ μm, $t_{m1} = 0.44$ μm, $a_2 = 18.5$ μm and $t_{m2} = 1.8$ μm again with $t_g = 0.25$ μm is

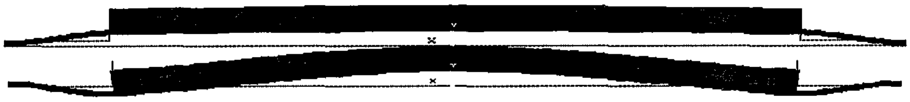

Figure 4.5: Modal shapes of the nonuniform membranae at f_r (upper one) and f_a (lower one).

simulated.

To investigate the effect of the nonuniform portion on f_r and f_a, we keep a_1 and t_{m1} constant at 40 μm and 0.8 μm, respectively. Fig. 4.6(a) shows the change of f_r and Fig. 4.6(b) shows f_a with respect to increasing t_{m2} for various a_2. The results indicate that for constant a_2 as t_{m2} is increased, f_r initially increases to reach a maximum value, then begins to decrease. This results in that nonuniform membrane will have the same f_r for two different t_{m2} values (denoted as first and second solutions). Referring to Fig. 2.5, in the first portion, the ruling effect is

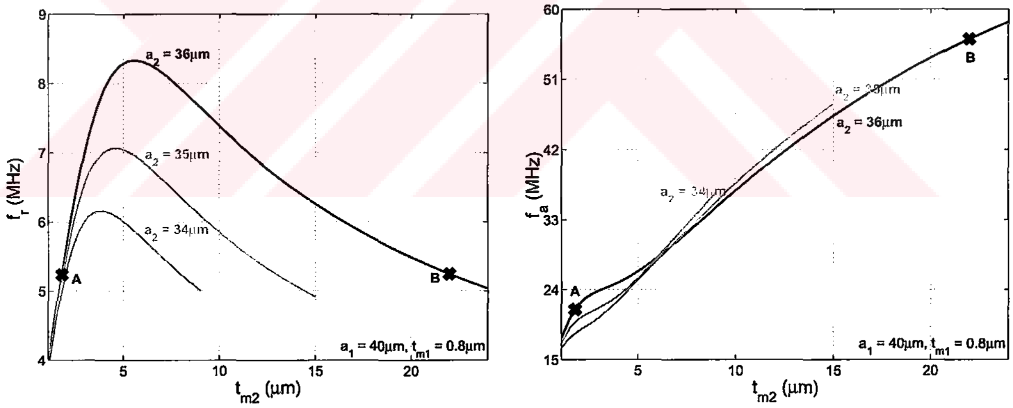

(a) (b)

Figure 4.6: Change of (a) f_r and (b) f_a with respect to t_{m2} for various a_2 when a_1 and t_{m1} are held constant at 40 μm and 0.8 μm.

the stiffness of the membrane and increasing t_{m2} can be considered as increasing the spring constant, k. At the second portion, the ruling effect is the mass of the membrane and increase in t_{m2} shows itself in the increase of the mass, m. As a_2 is increased, the maximum of f_r also increases. On the other hand, f_a

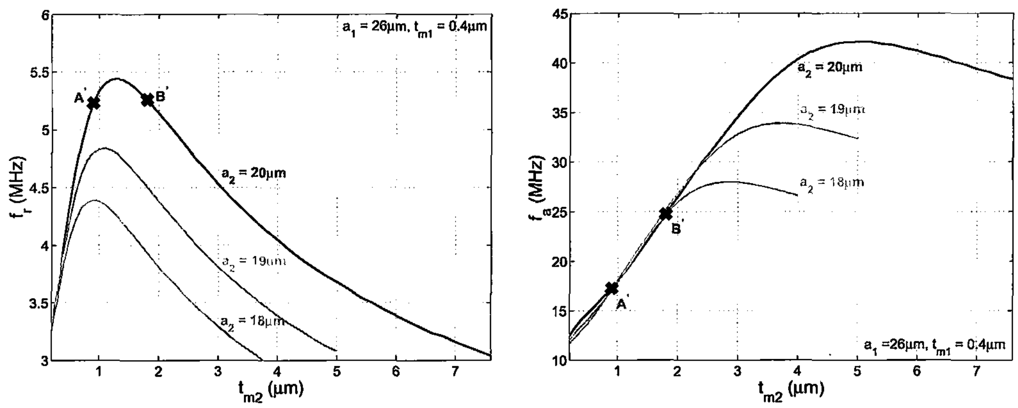

(a) (b)

Figure 4.7: Change of (a) f_r and (b) f_a with respect to t_{m2} for various a_2 when a_1 and t_{m1} are held constant at 26 μm and 0.4 μm.

continuously increases starting from around 15 MHz to 60 MHz. The points A (first solution) and B (second solution) in Fig. 4.6(a) have the same f_r, but the later one has a f_a of 60 MHz, showing the possibility of obtaining a bandwidth more than 50 MHz. The first solution shows a behavior similar to a uniform membrane, since t_{m2} value is small. On the other hand, second solution shows a piston like behavior due to high t_{m2}. The results are repeated for another a_1 - t_{m1} pair, 26 μm - 0.4 μm, can be seen in Fig. 4.7(a)-(b). Different from previous the configuration, a decrease in f_a is also seen after a critical t_{m2} value.

4.3 Receive Mode

In the receive mode, the input acoustic power is limited since the incoming wave is small in amplitude due to coming from another source or being reflected from a target. Hence it is important to use as much of the available acoustic power as possible. To obtain the best performance, the acoustic mismatch at the mechanical side (Fig. 3.1(a)) should be kept minimized. Similarly, the electrical mismatch at the electrical side should also be kept at minimum. For such a use, transducer power gain, G_T, definition is suited. It is given by [27]

$$G_T = \frac{\text{power delivered to the load}}{\text{available power from the source}} = \frac{P_L}{P_A}$$
$$= \frac{(1-|\Gamma_s|^2)}{|1-\Gamma_s\Gamma_{in}|^2}|S_{21}|^2\frac{(1-|\Gamma_L|^2)}{|1-S_{22}\Gamma_L|^2} \quad (4.1)$$

with

$$\Gamma_{in} = S_{11} + \frac{S_{21}S_{12}\Gamma_L}{1-S_{22}\Gamma_L} \quad (4.2)$$

Γ_L is the reflection coefficient at the load end and the corresponding s-parameters for cMUT is obtained from Mason's equivalent circuit. The highest transducer gain is obtained if the electrical side is complex conjugately matched to receiver impedance and the acoustic side is equal to the acoustic impedance of the immersion medium. The conversion gain is defined as the square root of the transducer power gain. Then, figure of merit for the receive mode, M_R, is defined as the product of the conversion gain and bandwidth [7];

$$M_R = \sqrt{G_T}B_2 \quad (4.3)$$

where B_2 is the 3-dB bandwidth of the transducer gain (Fig.4.8(a)).

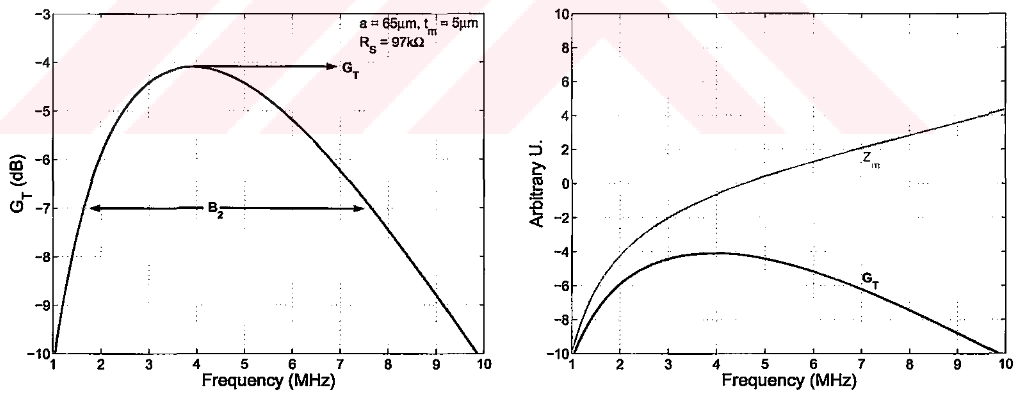

Figure 4.8: (a) Definition of figure of merit for the receive mode, M_R. (b) Transducer gain, G_T, and the mechanical impedance of the membrane, Z_m, (spring softening effect is included) with respect to frequency.

In Fig. 4.8(a), cMUT has an a and t_m of 65 μm and 5 μm and its f_r is 5.5 MHz[4].

[4]In this work, cMUTs having the same f_r are compared, since then they have approximately the same f_a, hence maximum amount of possible B_2.

t_g is 0.25 μm and the corresponding V_{col} is 118 V. 97 kΩ is used to terminate the electrical side of single cMUT. If N cMUTs were connected in parallel, 97/N kΩ will be required for termination[5]. From the small signal equivalent circuit, it is seen that the lower end of B_2, f_1, is determined by the RC network formed by R_S and C_0. On the other hand, f_2, the high frequency end of the B_2, is determined by Z_m(Fig.4.8(b)), since due to f_a, Z_m increases considerably resulting in the drop of G_T.

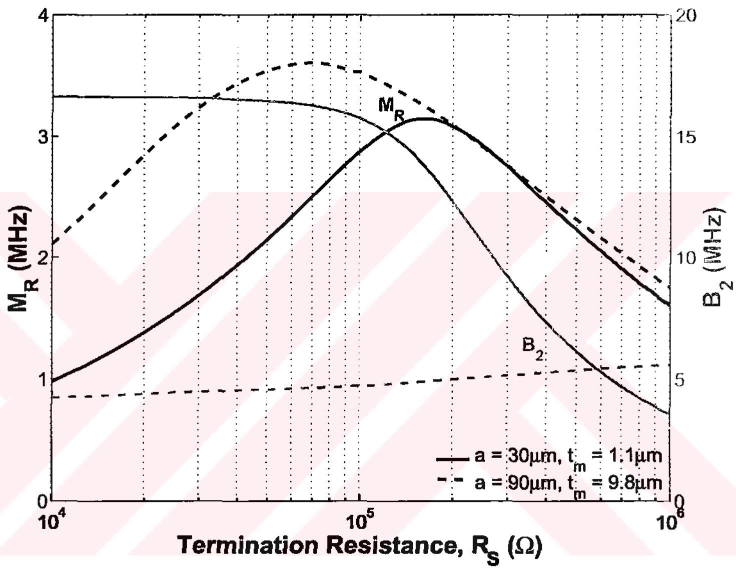

Figure 4.9: Change of M_R and B_2 with respect to R_S for a uniform membrane.

It is clear that the termination resistance, R_S, strongly affects G_T and B_2 by changing the Γ_{out} at the load side. It is possible to plot G_T and B_2 with respect to R_S (Fig. 4.9). Two cMUTs with different radiuses, 30 μm and 90 μm, but having the same f_r are simulated. The maximum value of M_R is reached at a certain R_S, showing the optimum point. However, more important than that, it is possible to operate cMUT different from the optimum point, by changing the R_S, with a considerably high bandwidth at the expense of reduced gain. Terminating the electrical side with 150 kΩ results in B_2 of 15 MHz and M_R of 3 MHz.

[5]In receive mode, all cMUTs are biased at %90 of their V_{col} and a small AC voltage is applied to find the equivalent circuit parameters.

A suitable electrode pattern for the uniform membranes has been proposed at the beginning of the chapter by investigating the change of the equivalent circuit parameters. It is also possible to look at the effect of the electrode radius on M_R. In Fig. 4.10, it is seen that B_2 is independent of the electrode radius. On the other hand, the decrease in C_0 results in the increase of G_T, however, at a certain point, the decrease in n (Fig. 4.1) can no longer be compensated by C_0 resulting in an optimum electrode radius, which gives the maximum M_R. In this thesis, we choose an electrode radius, which doesn't change the V_{col} and n rather than the optimum electrode radius.

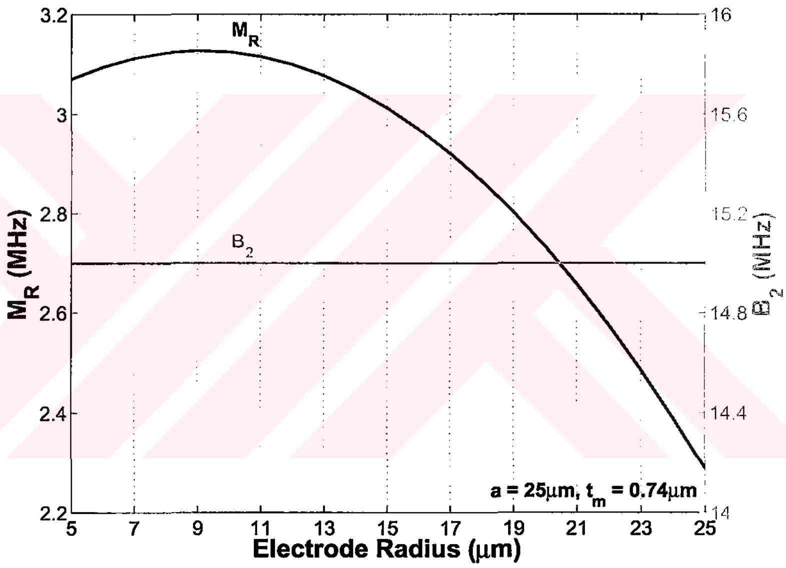

Figure 4.10: Change of M_R and B_2 with respect to electrode radius for a uniform membrane.

In [7], it is found that t_g has no effect on M_R except the change of the optimum R_S. In this work, all devices have a t_g of 0.25 μm. Fig. 4.11 shows the tradeoff between M_R and B_2. In this figure, a is changed and t_m values are chosen such that each a - t_m pair has an f_r of 5.5 MHz. Corresponding R_S values for termination are chosen to obtain the maximum M_R. This graph shows that with a particular choice of membrane dimensions, that cMUT shows the maximum performance when immersed in water, corresponding to a = 70 μm and t_m =

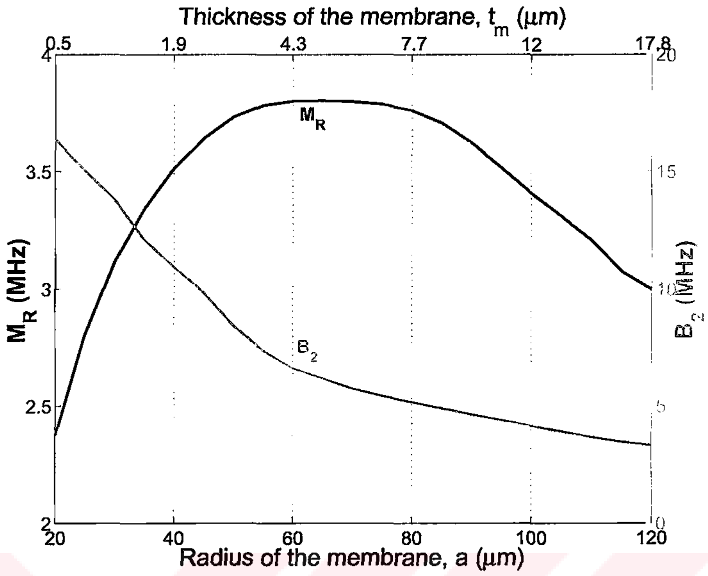

Figure 4.11: Change of M_R and B_2 with respect to a for a uniform membrane.

5 μm. For small values of a, Z_m is negligible compared to the acoustic impedance of water, hence the equivalent circuit simplifies to a simple RC network, with a high bandwidth but a low gain. However as a increases, B_2 begins to decrease but G_T increases. At the optimum point, the gain-bandwidth product, M_R, becomes 3.75 MHz and B_2 is 6 MHz.

Fig. 4.12(a) shows the calculated M_R and B_2 values with respect to R_S of nonuniform membranes shown as the points A and B in Fig. 4.6(a)-(b). As expected for point A, there is not much improvement in B_2, maximum of 15 MHz, since it shows a similar behavior to a uniform membrane. However, for point B, while expecting a B_2 around 50 MHz, a B_2 value of at most 4 MHz is obtained. This discrepancy, reduction in B_2, can be solved by recalling Fig. 4.8(b). We see that decrease in B_2 at high frequencies is due to the increased Z_m rather than f_a, which is a reason of that increase. However it is still possible to increase Z_m with other ways, such as increasing the mass of the membrane. This can also be seen in Fig. 4.12(b), which shows Z_m of points A and B. It is seen that although f_a of B is considerably higher than A, the value of Z_m is also high, even higher than Z_m of A around its f_a resulting in low B_2. Hence it is critical to be able to

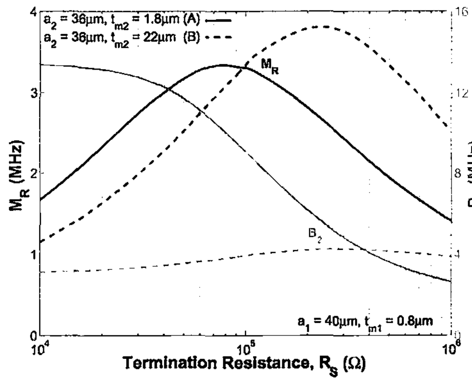

(a)

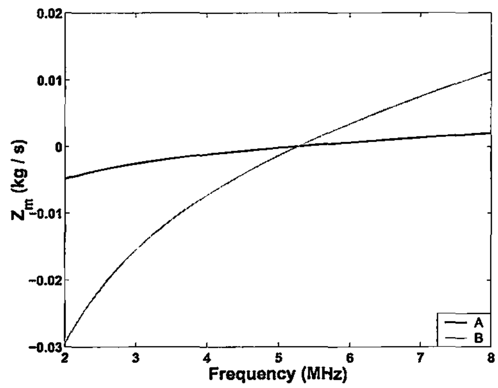

(b)

Figure 4.12: (a) Change of M_R and B_2 with respect to R_S for the nonuniform membranes denoted as A and B in Fig. 4.6(a). (b) Z_m of the points A and B (spring softening effect is not included).

increase f_a, without increasing Z_m value.

Nonuniform membrane fabricated with the sacrificial layer method is redrawn in Fig. 4.13. To keep Z_m as small as possible, one needs to keep the mass of the membrane small and to shift f_a to higher values, one needs to

- use smaller mass (smaller a_2 and t_{m2})
- use thinner uniform region (smaller t_{m1})
- keep the ratio, a_2/a_1 small (higher a_1)

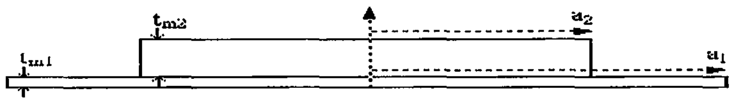

Figure 4.13: Nonuniform membrane fabricated with the sacrificial layer method.

The nonuniform membranes shown as the points A' and B' in Fig. 4.7(a)-(b) obeys the above considerations. The change of M_R and B_2 with respect to R_S can be seen in Fig. 4.14. As expected, point B' can have a B_2 of approximately

20 MHz. Also when R_S of 50 kΩ is used, cMUT will have a M_R of 3.2 MHz and B_2 of 19 MHz. It is important to note that the device dimensions, in terms of the thickness of the membrane, easily allows the fabrication of the devices with the current technology [15].

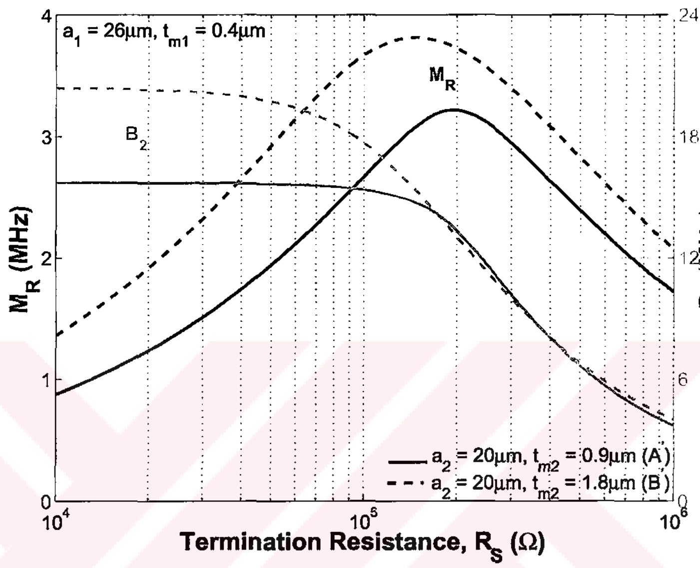

Figure 4.14: Change of M_R and B_2 with respect to R_S for the nonuniform membranes denoted as A' and B' in Fig. 4.7(a).

The effect of the electrode radius on M_R for a nonuniform membrane can be seen in Fig. 4.15. The optimum electrode radius is achieved if the electrode covers only the nonuniform region resulting maximum M_R. Similar to the uniform membrane case, it is possible to investigate the effect of membrane radius on M_R. To make such an investigation, we again keep the f_r of the membranes at 5.5 MHz and used the optimum R_S values for termination. Although there are many possible membrane configurations, we restrict ourselves choosing the membrane dimensions, also keeping in mind the requirements for low Z_m, such that a_2/a_1 ratio is equal to 0.75 and the ratio of t_{m1}/t_m[6] to 0.6. Since there are two t_{m2} values, first and second solutions, for the same f_r to occur, both of these solutions are plotted. Fig. 4.16(a) corresponds to the first solution and

[6] t_m corresponds to the required membrane thickness value if a uniform membrane is constructed with radius a_1 to resonate at the desired f_r.

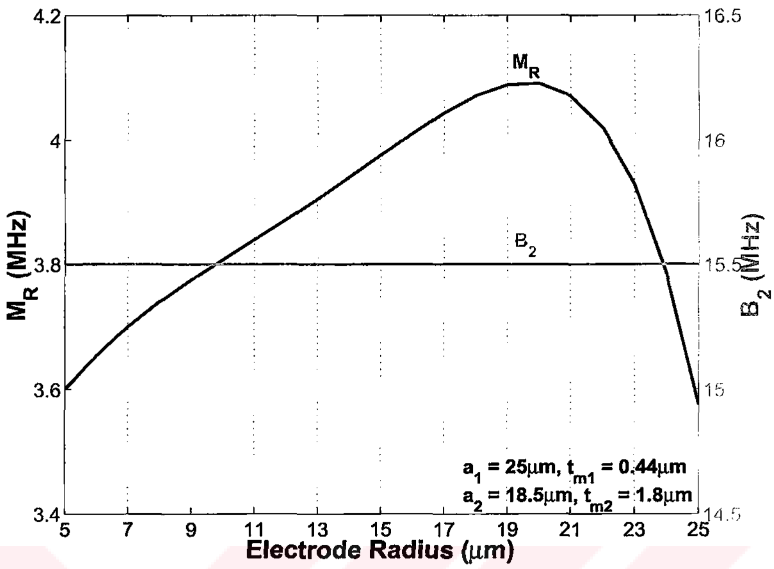

Figure 4.15: Change of M_R and B_2 with respect to electrode radius for a nonuniform membrane.

Fig. 4.16(b) corresponds to the second one. Since the first solution shows a similar behavior to a uniform membrane, there is not much improvement in B_2, however with the second solution B_2 can be as high as 20 MHz with a reasonably high gain. The optimum dimension for the maximum M_R is a_1, t_{m1}, a_2 and t_{m2} are equal to 45 μm, 1.44 μm, 33.5 μm and 4.8 μm. At that point M_R is 4.45 MHz and B_2 is 7 MHz.

4.4 Transmit Mode

During the transmission mode, there is no limitation in terms of the available power. Only limitation is the applied voltage due to the breakdown of the insulator material or V_{col} of the device. Referring to Fig. 3.1(b), it is important to maximize the pressure, P, at the mechanical side, which is given by $P = F/S$. Let B_1 be the associated 3-dB bandwidth, then the figure of merit for the transmit

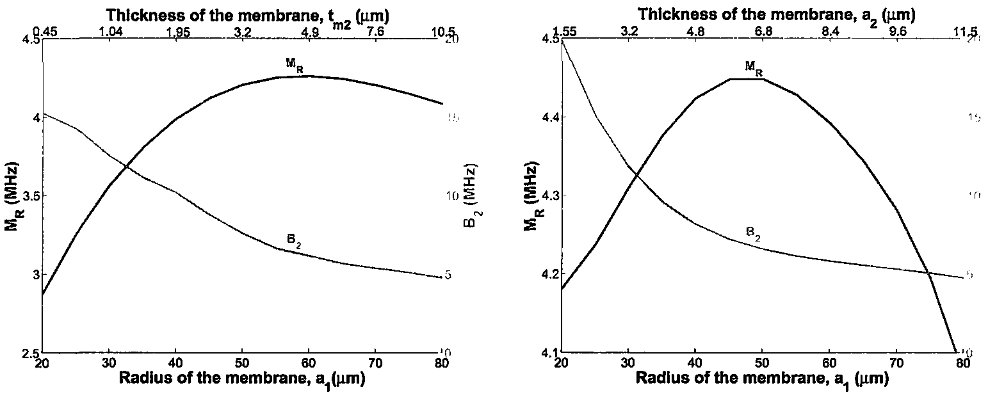

(a) (b)

Figure 4.16: Change of M_R and B_2 with respect to a_1 corresponding to the (a) first solution. (b) second solution.

mode can be defined as (Fig. 4.17)

$$M_T = PB_1 \tag{4.4}$$

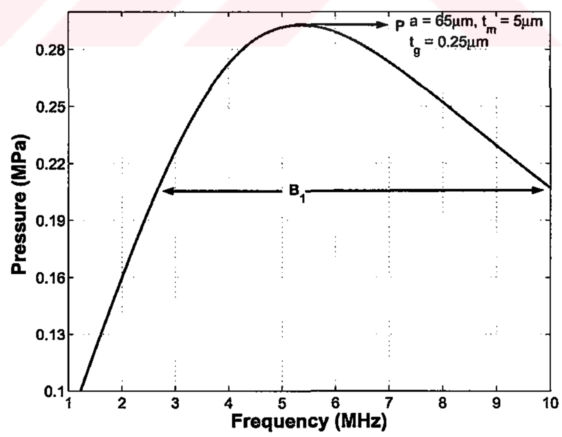

Figure 4.17: Definition of figure of merit for the transmit mode.

While calculating the equivalent circuit parameters, the maximum peak voltage on the electrode is assumed to be 0.9 of V_{col} and cMUT is biased at 0.45

of V_{col}. Higher order harmonics generated during the transmission is neglected. Change of M_T with respect to the electrode radius can be seen in Fig. 4.18(a). B_1 is independent of the electrode radius, however, M_T continuously decreases. However, at the point, where the electrode covers %70 of the membrane, degradation is not much, still suitable for use. Fig. 4.18(b) shows the change of M_T and B_1 of the uniform membrane with respect to a. Again t_m values are chosen to have an f_r of 5.5 MHz. In [7], B_1 is shown to be independent of t_g, however, M_T increases as t_g increases, since the maximum applied voltage also increases. cMUTs with smaller a have higher B_1, but lower M_T. As a is increased, M_T increases but B_1 decreases. The maximum achievable M_T for a t_g of 0.25 μm is 2.2 MPa MHz. With an a and t_m of 60 μm and 4.3 μm, it is possible to obtain a B_1 of approximately 8 MHz.

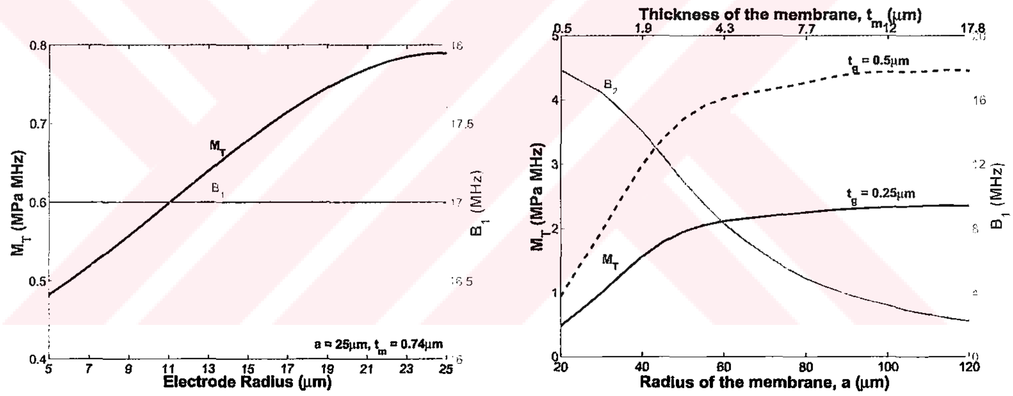

(a) (b)

Figure 4.18: (a) Change of M_T and B_1 with respect to the electrode radius. (b) Change of M_T and B_1 with respect to a for a uniform membrane.

Similar to the uniform membrane, we can look at the performance of the nonuniform membranes with respect to the electrode radius (Fig. 4.19(a)). Again when the electrode covers only the nonuniform region, there is not much degradation in terms of M_T.

We can look at the performance of the nonuniform membranes in the first and second solution regions. Same membrane dimensions used in Fig. 4.16 are used. The results can be seen in Fig. 4.19.

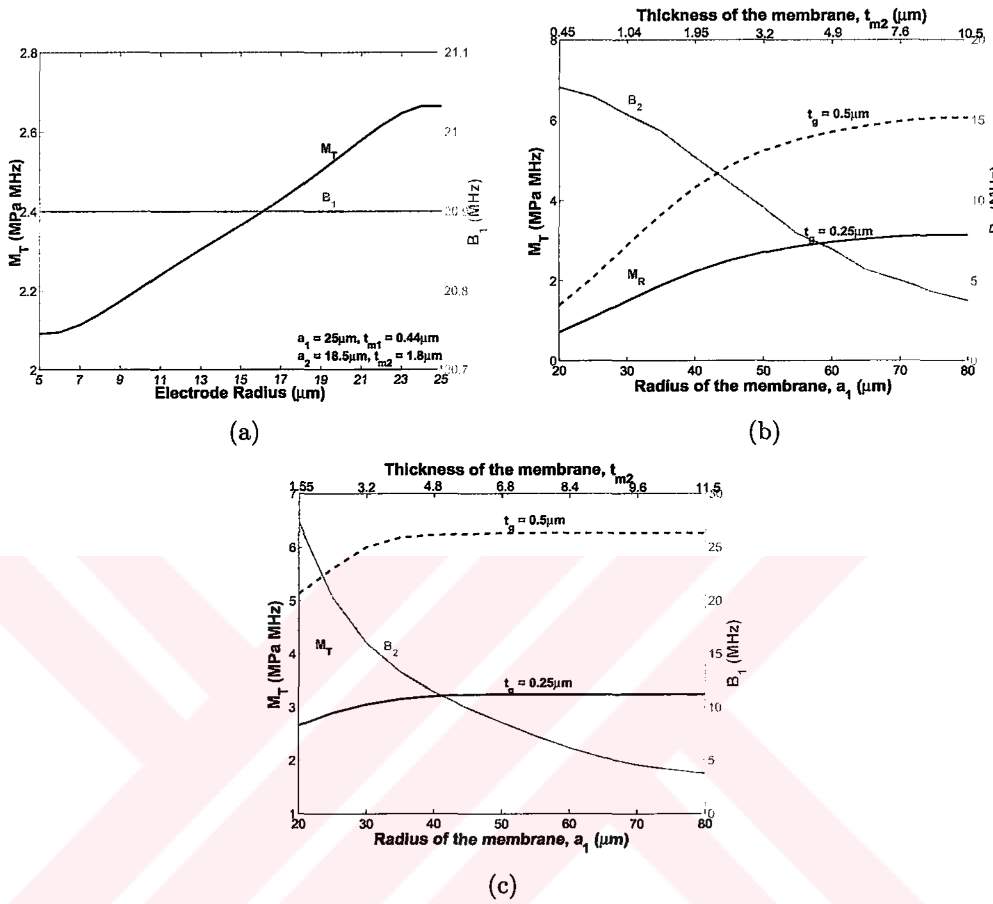

Figure 4.19: Change of M_T and B_1 with respect to (a) the electrode radius (b) a_1 corresponding to the first solution. (c) a_1 corresponding to the second solution.

As it can be seen from Fig. 4.19(c), it is possible to obtain high B_1 and M_T with the same cMUT, which is not possible with a uniform membrane.

Chapter 5

CONCLUSION

Capacitive micromachined ultrasonic transducer (cMUT) offers high bandwidth in low impedance media at the expense of low gain due to their low turns ratio. A recent work [7] showed that a cMUT immersed in water can be optimized for both high gain and bandwidth for a given frequency range.

In this work, by using the performance measures in [7], it is shown that low gain of the cMUT is due to low turns ratio and the bandwidth of the device is limited by the antiresonance frequency of the membrane. A nonuniform membrane is proposed to increase the turns ratio of the device and shift the antiresonance frequency of the membrane to higher values.

First a suitable electrode pattern, which decreases the shunt input capacitance, but doesn't change the collapse voltage and turns ratio, is found. Then the change of natural resonance and antiresonance frequencies of uniform and nonuniform membranes for different configurations is investigated. Although more that %200 increase in the antiresonance frequency without changing the natural resonance frequency is obtained for a nonuniform membrane, it is also shown that shifting the antiresonance is not enough. To obtain high bandwidth, one also needs to decrease the membrane impedance. For a suitable nonuniform membrane configuration, the results are obtained for both receive and transmit modes. It is shown that without increasing the membrane impedance, it is possible to increase the antiresonance frequency %40. Various designs having high bandwidth and considerably high gain is presented. The membrane configurations are compared for both receive and transmit modes and it is shown that use of nonuniform membranes are advantageous in many aspects.

Future work must include the analytic modeling of the nonuniform membranes, since it may be time consuming to perform finite element simulations for each configurations for different operation modes to obtain an optimum design. A good starting point will be the first order electromechanical model (Fig. 2.5) introduced in chapter 2.

Appendix A

A.1 Solution Of Mason's Differential Equation

The equation,

$$\frac{(Y_0 + T)t_m^3}{12(1-\sigma^2)}\nabla^4 y(r) - t_m T \nabla^2 y(r) - P - \omega^2 t_m \rho y(r) = 0 \tag{A.1}$$

is known to have a solution of the form

$$y(r) = AJ_0(k_1 r) + BJ_0(k_2 r) + CY_0(k_1 r) + DY_0(k_2 r) - \frac{P}{\omega^2 t_m \rho} \tag{A.2}$$

where $J_0()$ is the zeroth order Bessel function of the first kind and $Y_0()$ is the zeroth order Bessel function of the second kind with arbitrary constants A, B, C and D. Since $r = 0$ is the singular point of $Y_0()$ which leads to physically unrealistic solution; we deduce that $C = D = 0$.

In polar coordinates using symmetry (no variation on ϕ); the Laplacian operator is equal to,

$$\nabla^2 y(r) = \frac{\mathrm{d}^2 y(r)}{\mathrm{d}r^2} + \frac{1}{r}\frac{\mathrm{d}y(r)}{\mathrm{d}r} \tag{A.3}$$

and for $x(r) = AJ_0(kr)$, we obtain

$$\nabla^2 y(r) = \nabla^2(AJ_0(kr)) = -Ak^2 J_0(kr) \tag{A.4}$$

Similarly the Bilaplacian operator is,

$$\nabla^4 y(r) = \frac{\mathrm{d}^4 y(r)}{\mathrm{d}r^4} + \frac{2}{r}\frac{\mathrm{d}^3 y(r)}{\mathrm{d}r^3} - \frac{1}{r^2}\frac{\mathrm{d}^2 y(r)}{\mathrm{d}r^2} + \frac{1}{r^3}\frac{\mathrm{d}y(r)}{\mathrm{d}r} \tag{A.5}$$

and for $x(r) = AJ_0(kr)$,

$$\nabla^4 y(r) = \nabla^4(AJ_0(kr)) = Ak^4 J_0(kr) \tag{A.6}$$

If we plug (A.2) in (A.1); we obtain the characteristic equation,

$$\frac{(Y_0+T)t_m^2}{12(1-\sigma^2)\rho}k_{1,2}^4 + \frac{T}{\rho}k_{1,2}^2 - \omega^2 = 0 \tag{A.7}$$

Following Mason's notation; define

$$c = \frac{(Y_0+T)t_m^2}{12(1-\sigma^2)\rho}\ ,\ d = \frac{T}{\rho} \tag{A.8}$$

then the solution to A.7 is,

$$\begin{aligned} k_{1,2}(1) =& \sqrt{\frac{-d+\sqrt{d^2+4c\omega^2}}{2c}} \text{ and } k_{1,2}(2) = -\sqrt{\frac{-d+\sqrt{d^2+4c\omega^2}}{2c}} \\ k_{1,2}(3) =& j\sqrt{\frac{d+\sqrt{d^2+4c\omega^2}}{2c}} \text{ and } k_{1,2}(4) = -j\sqrt{\frac{d+\sqrt{d^2+4c\omega^2}}{2c}} \end{aligned} \tag{A.9}$$

Since $J_0(-x) = J_0(x)$; let's choose the roots with the positive signs.

We need two boundary conditions to determine A and B, which are

$$\begin{aligned} y(r)|_{r=a} = 0 &\Longrightarrow AJ_0(k_1a) + BJ_0(k_2a) = \frac{P}{\omega^2 l_t \rho} \\ \left.\frac{\mathrm{d}y(r)}{\mathrm{d}r}\right|_{r=a} = 0 &\Longrightarrow Ak_1J_1(k_1a) + Bk_2J_1(k_2a) = 0 \end{aligned} \tag{A.10}$$

After the determination of the constants, $y(r)$ is given by

$$y(r) = \frac{P}{\omega^2 t_m \rho}\left[\frac{-k_2J_1(k_2a)J_0(k_1r) + k_1J_1(k_1a)J_0(k_2r)}{-k_2J_1(k_2a)J_0(k_1a) + k_1J_1(k_1a)J_0(k_2a)} - 1\right] \tag{A.11}$$

The velocity of the membrane is $v(r) = j\omega y(r)$; then the average velocity, $\overline{v}$, is the integration of this velocity over whole membrane divided by area, $S = \pi a^2$, which is

$$\overline{v} = \frac{1}{\pi a^2}\int_0^{2\pi}\int_0^a v(r)r\mathrm{d}r\mathrm{d}\theta = \frac{j\omega}{\pi a^2}\int_0^{2\pi}\int_0^a y(r)r\mathrm{d}r\mathrm{d}\theta \tag{A.12}$$

using the identity $\int xJ_0(\alpha x)\mathrm{d}x = \frac{1}{\alpha}xJ_1(\alpha x)$; we obtain

$$\begin{aligned} \overline{v} =& \frac{jP2}{a^2\omega l_t\rho}\left[\frac{-k_2J_1(k_2a)J_1(k_1r)r}{(-k_2J_1(k_2a)J_0(k_1a) + k_1J_1(k_1a)J_0(k_2a))k_1} + \right. \\ & \left.\left.\frac{k_1J_1(k_1a)J_1(k_2r)r}{(-k_2J_1(k_2a)J_0(k_1a) + k_1J_1(k_1a)J_0(k_2a))k_2} - \frac{r^2}{2}\right]\right|_0^a \end{aligned} \tag{A.13}$$

Finally, the average velocity is given by

$$\overline{v} = \frac{jP}{\omega l_t \rho}\Big[\frac{2(k_1^2 - k_2^2)J_1(k_1 a)J_1(k_2 a)}{ak_1k_2(-k_2J_1(k_2a)J_0(k_1a) + k_1J_1(k_1a)J_0(k_2a))} - 1\Big] \tag{A.14}$$

And by definition, the mechanical impedance is given by the uniform pressure, P, applied to the membrane divided by average velocity, $\overline{v}$. Hence Z_m is

$$\begin{aligned} Z_m &= \frac{P}{\overline{v}} \\ &= j\omega l_t \rho \Big[\frac{ak_1k_2(-k_2J_1(k_2a)J_0(k_1a) + k_1J_1(k_1a)J_0(k_2a))}{ak_1k_2(-k_2J_1(k_2a)J_0(k_1a) + k_1J_1(k_1a)J_0(k_2a)) - 2(k_1^2 - k_2^2)J_1(k_1a)J_1(k_2a)}\Big] \end{aligned} \tag{A.15}$$

A.2 Derivation Of Operation Parameters

The capacitance between the electrodes is the series combination of three capacitances; namely membrane, gap and insulator (Fig. 2.3). These three capacitances can be written in the differential form as

$$dC_m = \frac{\epsilon_m}{t_e}ds \text{ , } dC_g = \frac{\epsilon_0}{t_g - y(r)}ds \text{ and } dC_i = \frac{\epsilon_i}{t_i}ds \tag{A.16}$$

Series combination of these differential capacitances is given by

$$\begin{aligned} dC_0 &= \frac{dC_m dC_g dC_i}{dC_m dC_g + dC_m dC_i + dC_g dC_i} \\ &= \frac{\epsilon_0 \epsilon_{rm} \epsilon_{ri}}{\epsilon_{rm} t_i + \epsilon_{rm}\epsilon_{ri}(t_g - y(r)) + \epsilon_{ri} t_e} ds \end{aligned} \tag{A.17}$$

The total capacitance is equal to the integration of the differential capacitance over whole area, which is

$$\begin{aligned} C_0 &= \int_0^{2\pi}\int_0^{a+t_{eff}} \frac{\epsilon_0 \epsilon_{rm} \epsilon_{ri}}{\epsilon_{rm} t_i + \epsilon_{rm}\epsilon_{ri}(t_g - y(r)) + \epsilon_{ri} t_e} r dr d\theta \\ &\simeq \frac{S' \epsilon_0 \epsilon_{rm} \epsilon_{ri}}{\epsilon_{rm} t_i + \epsilon_{rm}\epsilon_{ri} t_{g0} + \epsilon_{ri} t_e} \end{aligned} \tag{A.18}$$

where S' is the area of the membrane with extended radius to include the fringing fields. Approximation is performed under the assumption that all points of membrane deflected at the same amount, which is $t_g - t_{g0}$.

Second step is to derive the turns ratio, n. Again referring to Fig. 2.3, total current, I, flowing through cMUT under operation is given by

$$I = \frac{dQ}{dt} = \frac{d}{dt}\Big(C(t)V(t)\Big) = C(t)\frac{dV(t)}{dt} + V(t)\frac{dC(t)}{dt} \tag{A.19}$$

where $V(t)$ is the total applied voltage and $C(t)$ is the time variable capacitance. Under the small signal approximation; we can separate the static and dynamic parts of $V(t)$ and $C(t)$ as; $V(t) = V_{DC} + V_{AC}\sin(\omega t)$ and $C(t) = C_0 + C_{AC}\sin(\omega t + \phi)$ with $V_{AC} \ll V_{DC}$ and $C_{AC} \ll C_0$. Then (A.19) can be approximated as

$$I \approx C_0\frac{dV_{AC}(t)}{dt} + V_{DC}\frac{dC_{AC}(t)}{dt} \tag{A.20}$$

When the time derivative for C_{AC} is calculated

$$\begin{aligned} I &\approx C_0\frac{dV_{AC}(t)}{dt} - \underbrace{V_{DC}\frac{S\epsilon_0(\epsilon_{rm}\epsilon_{ri})^2}{(\epsilon_{rm}t_i + \epsilon_{rm}\epsilon_{ri}t_{g0} + \epsilon_{ri}t_e)^2}}_{n}\underbrace{\frac{dt_g(t)}{dt}}_{\overline{v}} \\ &\approx C_0\frac{dV_{AC}(t)}{dt} - n\overline{v} \end{aligned} \tag{A.21}$$

where $dt_g(t)/dt$ is the average velocity of the membrane. (A.21) shows the conversion of a mechanical quantity, $\overline{v}$, to an electrical quantity, I. Then n is

$$n = \frac{S'\epsilon_0(\epsilon_{rm}\epsilon_{ri})^2}{(\epsilon_{rm}t_i + \epsilon_{rm}\epsilon_{ri}t_{g0} + \epsilon_{ri}t_e)^2}V_{DC} \tag{A.22}$$

Last step is to find V_{col}. First order model shown in Fig. 2.5 is suited for calculation. The accelerating force exerted by the mass is $F_{mass} = m\ddot{y}(r,t)$ and the restoring force of the spring is $F_{spring} = -ky(r,t)$. The electrostatic force exerted by the capacitor under constant voltage assumption is

$$\begin{aligned} F_E =& \frac{\mathrm{d}W_e}{\mathrm{d}y(r,t)} = \frac{\mathrm{d}}{\mathrm{d}y(r,t)}\Big(\frac{1}{2}CV^2\Big) = \frac{V^2}{2}\frac{\mathrm{d}C}{\mathrm{d}y(r,t)} \\ =& -\frac{1}{2}\frac{S\epsilon_0(\epsilon_{rm}\epsilon_{ri})^2}{(\epsilon_{rm}t_i + \epsilon_{rm}\epsilon_{ri}(t_g - y(r,t)) + \epsilon_{ri}t_e)^2}V^2 \end{aligned} \tag{A.23}$$

The sum of these three forces will be 0 at the equilibrium, hence

$$\begin{aligned} F_N =& F_{mass} - F_E - F_{spring} \\ & m\frac{\partial^2 y(r,t)}{\partial t^2} - \frac{1}{2}\frac{S\epsilon_0(\epsilon_{rm}\epsilon_{ri})^2}{(\epsilon_{rm}t_i + \epsilon_{rm}\epsilon_{ri}(t_g - y(r,t)) + \epsilon_{ri}t_e)^2}V^2 + ky(r,t) = 0 \end{aligned} \tag{A.24}$$

Since DC behavior is considered, time derivative term can be set to 0; to obtain (time and spatial dependence have been left out)

$$F_N = ky - \frac{1}{2}\frac{S\epsilon_0(\epsilon_{rm}\epsilon_{ri})^2}{(\epsilon_{rm}t_i + \epsilon_{rm}\epsilon_{ri}(t_g - y) + \epsilon_{ri}t_e)^2} = 0 \tag{A.25}$$

The membrane collapses when the derivative of F_N is set to 0 showing the unstable behavior of membrane. The inflection displacement is

$$y(r)|_{r=0} = \frac{t_{eff}}{3} \tag{A.26}$$

where the effective gap height, t_{eff} is

$$t_{eff} = t_g + \frac{\epsilon_{rm}t_i + \epsilon_{ri}t_e}{\epsilon_{rm}\epsilon_{ri}} \tag{A.27}$$

and at that point collapse voltage, V_{col}, is

$$V_{col} = \sqrt{\frac{128Y_0t_m^3t_{eff}^3}{36\epsilon_0(1-\sigma^2)a^4}} \tag{A.28}$$

Appendix B

Finite Element Simulation

ANSYS^{TM} 8.1, a commercially available finite element package, is used in simulations. The simulations are composed of two parts. The first part, static analysis, yields the deflected membrane shape, shunt input capacitance (C_O) and DC electric fields used in the second step for an applied DC voltage. The second part, dynamic analysis, yields the mechanical impedance of the membrane (Z_m) and turns ratio (n).

Structural and electrostatic regions are modeled with $PLANE82$ and $PLANE121$ elements [28]. An infinitely small thickness metal electrode is assumed instead of putting a full thickness metal electrode, which doesn't effect the results considerably [25]. $TARGE169$-$CONTA172$ element pair is used for the contact region that forms between the membrane and insulator when membrane collapses. The model is meshed with quadrilateral elements except the gap, which is meshed with triangles for re-meshing ease. For all elements, axis-symmetric option is enabled which denotes 360^0 rotation around the symmetry axis that passes through the center. Hence only the cross-section of the structure is modeled.

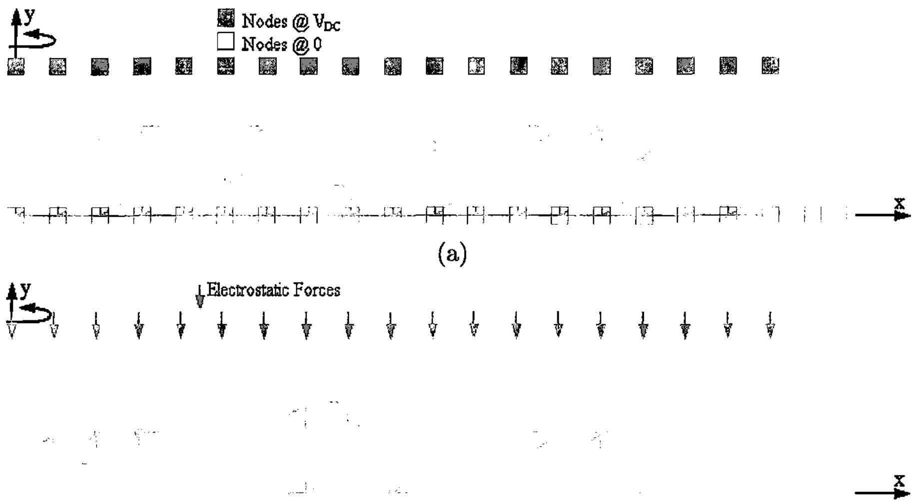

(a) (b)

Figure B.1: Application of (a) voltages and (b) electrostatic forces to FEM

B.1 Static Analysis

When a voltage is applied to the membrane, resulting electrostatic fields hence the forces can be solved. When those forces are applied to the membrane, it will deflect towards the insulator. However such a deflection will call a change in electrostatic fields and forces. So the electrostatic problem must be resolved for this new configuration, which must be followed by another structural analysis [29]. This iterative process will continue until a convergence criterion depending on the choice is reached. The following part summarizes the steps for the solution of membrane operating in the conventional regime.

- V_{DC} is applied to each node on the electrode (Fig. B.1(a)).
- Resulting electric field due to the voltage distribution is solved. (Electrostatic problem)
- The electric field underneath the electrode is squared and multiplied with

Maxwell Stress Tensor coefficient to find the electrostatic forces[1] The coefficient for the top and bottom electrode cases is given by

$$MSTc = \frac{\epsilon_m^2}{2\epsilon_0} \text{ and } MSTc = \frac{\epsilon_0}{2} \tag{B.1}$$

and the applied electrostatic force is

$$F_{DC}(r) = -\mathbf{a_y}\frac{\epsilon_m^2}{2\epsilon_0}E_{DC}^2(r) \text{ and } F_{DC}(r) = -\mathbf{a_y}\frac{\epsilon_0}{2}E_{DC}^2(r) \tag{B.2}$$

- The electrostatic forces are applied to each node on the electrode of undeflected membrane (Fig. B.1(b)).
- The deflection of the membrane for the applied forces are solved (Structural problem) and the finite element model is re-meshed according to the deflections given by the solution.
- Since the shape of the structure is changed, the electrostatic problem is also altered. Hence electrostatic problem must be resolved. So turn back to 1^{st} step.
- The above steps are remade until a convergence criterion depending on the choice is reached. The convergence criterion in the simulations is chosen to be the change in maximum displacement difference between the previous iteration' is 0.002 of previous iteration's maximum displacement.

When cMUT is operating in the collapse mode, the above steps are modified as follows:

- The center of the membrane is initially displaced to %5 of t_g, such an offset is necessary to re-mesh the vacuum region between the iterations and it only increases the effective thickness of the insulator [25]. Hence a contact between $TARGE169$ and $CONTA172$ elements forms. The resulting structural problem is solved and the new finite element model is formed.

[1] For more detailed derivation of Maxwell Stress Tensor coefficient and electrostatic forces, reader is advised to refer to [29, 30].

- The other steps are same as in conventional regime except the use of new finite element model.
- The convergence criteria is chosen to be the stored electrostatic energy

$$W_e = \frac{1}{2} C_0 V_{DC}^2 \tag{B.3}$$

difference between the previous solution is 0.002 of electrostatic energy obtained in previous solution.

C_0 is extracted using $CMATRIX$ macro of ANSYS [31, 32].

B.2 Dynamic Analysis

In dynamic analysis, two separate harmonic analysis are performed. In the first part, Z_m is found. By following Eq. A.15, a uniform pressure, P, small in amplitude is applied; then the resulting average velocity, $\overline{v}$, is calculated. Z_m is given by $P/\overline{v}$.

Second step is to find n. V_{AC} is applied to electrode of deflected membrane and E_{AC} is solved. Then by using the same approach in static analysis, F_{AC} is calculated and applied to electrode. Since the transducers are assumed to have reduced electrodes (electrode doesn't cover the whole membrane); it is reasonable to define an effective force, which is

$$F_{effective}(\omega) = \overline{v} Z_m(\omega) \tag{B.4}$$

then; n is

$$n = \frac{F_{effective}(\omega)}{V_{AC}} \tag{B.5}$$

For effective used of applied voltage, in all simulations the electrode is assumed to be at the bottom of the membrane. However for meshing ease, the electrode is put $0.1\mu m$ away the vacuum-membrane interface.

Appendix C

MATERIAL PARAMETERS

The following is the material properties of materials used in the simulations.

Material	E (GPa)	ρ (kg/m^3)	σ $(unitless)$	ϵ/ϵ_0 $(unitless)$
Vacuum				1
Silicon	169	2332	0.278	11.8
Silicon Nitride	320	3270	0.263	5.7

E	Young's modulus
ρ	Mass density
σ	Poisson's ratio
ϵ/ϵ_0	Relative permittivity

Bibliography

[1] B. Bayram, E. Hæggström, G. G. Yaralioglu, and B. T. Khuri-Yakub, "A new regime for operating capacitive micromachined ultrasonic transducers," *IEEE Transactions on Ultrasonics, Ferroelectrics, and Frequency Control*, vol. 50, no. 9, pp. 1184 – 1190, 2003.

[2] D. Ensminger, *Ultrasonics.* New York: Marcel Dekker, Inc., 1988.

[3] J. D. N. Cheeke, *Fundamentals and Applications of Ultrasonic Waves.* Florida: CRC Press, 2002.

[4] G. S. Kino, *Acoustic Waves: Devices, Imaging, and Analog Signal Processing.* New Jersey: Prentice-Hall, Inc., 1987.

[5] http://www.morganelectroceramics.com.

[6] M. I. Haller and B. T. Khuri-Yakub, "A surface micromachined electrostatic ultrasonic air transducer," in *IEEE Ultrasonics Symposium*, 1994.

[7] S. Olcum, M. N. Senlik, and A. Atalar, "Optimization of the gain-bandwidth product of capacitive micromachined ultrasonic transducer," *IEEE Transactions on Ultrasonics, Ferroelectrics, and Frequency Control*, to be published.

[8] I. Ladabaum, X. Jin, H. T. Soh, A. Atalar, and B. T. Khuri-Yakub, "Surface micromachined capacitive ultrasonic transducers," *IEEE Transactions on Ultrasonics, Ferroelectrics, and Frequency Control*, vol. 45, no. 3, pp. 1364 – 1374, 1998.

[9] O. Oralkan, A. S. Ergun, J. A. Johnson, M. Karaman, U. Demirci, K. Kaviani, T. H. Lee, and B. T. Khuri-Yakub, "Capacitive micromachined ultrasonic transducers: Next-generation arrays for acoustic imaging," *IEEE Transactions on Ultrasonics, Ferroelectrics, and Frequency Control*, vol. 49, no. 11, pp. 1596 – 1610, 2002.

[10] O. Oralkan, A. S. Ergun, C. H. Cheng, J. A. Johnson, M. Karaman, T. H. Lee, and B. T. Khuri-Yakub, "Volumetric ultrasound imaging using 2-d cmut arrays," *IEEE Transactions on Ultrasonics, Ferroelectrics, and Frequency Control*, vol. 50, no. 11, pp. 1581 – 1594, 2003.

[11] G. G. Yaralioglu, A. S. Ergun, B. Bayram, E. Hæggström, and B. T. Khuri-Yakub, "Calculation and measurement of electromechanical coupling coefficient of capacitive micromachined ultrasonic transducers," *IEEE Transactions on Ultrasonics, Ferroelectrics, and Frequency Control*, vol. 50, no. 4, pp. 449 – 456, 2003.

[12] X. Jin, O. Oralkan, F. L. Degertekin, and B. T. Khuri-Yakub, "Fabrication and characterization of surface micromachined ultrasonic immersion transducer," *IEEE Transactions on Ultrasonics, Ferroelectrics, and Frequency Control*, vol. 48, no. 3, pp. 750 – 760, 2001.

[13] X. Jin, I. Ladabaum, and B. T. Khuri-Yakub, "The microfabrication of capacitive ultrasonic transducers," *Journal of Micromechanical Systems*, vol. 7, no. 3, pp. 295 – 302, 1998.

[14] X. Jin, I. Ladabaum, , F. L. Degertekin, S. Calmes, and B. T. Khuri-Yakub, "Fabrication and characterization of surface micromachined ultrasonic immersion transducer," *IEEE Journal of Microelectromechanical Systems*, vol. 8, no. 1, pp. 100 – 114, 1999.

[15] Y. Huang, A. S. Ergun, Edward, M. H. Badi, and B. T. Khuri-Yakub, "Fabricating capacitive micromachined ultrasonic transducers with wafer-bonding technology," *Journal of Micromechanical Systems*, vol. 12, no. 2, pp. 128 – 137, 2003.

[16] B. Bayram, E. Hæggström, A. S. Ergun, G. G. Yaralioglu, and B. T. Khuri-Yakub, "Dynamic analysis of cmuts in different regimes of operation," in *IEEE Ultrasonics Symposium*, 2003.

[17] W. P. Mason, *Electromechanical Transducers and Wave Filters*, 2nd ed. New York: D. Van Nostrand Company, Inc., 1948.

[18] M. H. Badi, "Capacitive micromachined ultrasonic lamb wave transducers," Ph.D. dissertation, Stanford University, 2004.

[19] M. Rossi, *Acoustics And Electroacoustics.* Norwood, MA: Artech House, 1988.

[20] G. T. A. Kovacs, *Micromachined Transducers Sourcebook.* New York: McGraw-Hill Book Company, Inc., 1998.

[21] H. A. C. Tilmans, "Equivalent circuit representation of electromechanical transducers: I. lumped-parameter systems," *Journal of Micromechanics and Microengineering*, vol. 6, pp. 157 – 176, 1996.

[22] G. G. Yaralioglu, M. H. Badi, A. S. Ergun, and B. T. Khuri-Yakub, "Improved equivalent circuit and finite element method modeling of capacitive micromachined ultrasonic transducer," in *IEEE Ultrasonics Symposium*, 2003.

[23] A. Lohfink, P.-C. Eccardt, W. Benecke, and H. Meixner, "Derivation of a 1d cmut model from fem results for linear and nonlinear equivalent circuit simulation," in *IEEE Ultrasonics Symposium*, 2003.

[24] F. Wen, W. Li, Q. Huang, and H. Rong, "Large-signal lumped-parameter macromodels for the equivalent circuit representation of electromechanical transducers," *Journal of Micromechanics and Microengineering*, vol. 14, pp. 452 – 461, 2004.

[25] B. Bayram, G. G. Yaralioglu, A. S. Ergun, and B. T. Khuri-Yakub, "Influence of the electrode size and location on the performance of a cmut," in *IEEE Ultrasonics Symposium*, 2001.

[26] A. Bozkurt, I. Ladabaum, A. Atalar, and B. T. Khuri-Yakub, "Theory and analysis of electrode size optimization for capacitive microfabricated ultrasonic transducers," *IEEE Transactions on Ultrasonics, Ferroelectrics, and Frequency Control*, vol. 46, no. 6, pp. 1364 – 1374, 1999.

[27] R. Ludwig and P. Bretchko, *RF Circuit Design: Theory and Applications.* New Jersey: Prentice-Hall, Inc., 2000.

[28] *ANSYS Element Reference*, ANSYS User Manual, 2004.

[29] A. Bozkurt, "Modeling and characterization of capacitive micromachined ultrasonic transducers," Ph.D. dissertation, Bilkent University, 2000.

[30] R. Plonsey and R. E. Collin, *Principles and Applications of Electromagnetic Fields.* New York: McGraw-Hill Book Company, Inc., 1961.

[31] *ANSYS Command Reference*, ANSYS User Manual, 2004.

[32] *ANSYS Theory Reference*, ANSYS User Manual, 2004.